FERROELECTRIC TUNGSTEN BRONZE BULK CRYSTALS AND EPITAXIAL THIN FILMS FOR ELECTRO-OPTIC DEVICE APPLICATIONS

Semi-Annual Technical Report No. 2
For Period 4/1/83 through 9/30/83

FEBRUARY 1984

DARPA Order No.	4540
Program Code:	P2D10
Name of Contractor	Rockwell International Corporation
Effective Date of Contract:	09/30/82
Contract Expiration Date:	09/29/85
Amount of Contract Dollars:	$1,051,699
Contract Number	N00014-82-C-2466
Principal Investigators:	Dr. R.R. Neurgaonkar (805) 498-4545, Ext. 109
	Dr. L.E. Cross Pennsylvania State University (814) 865-1181

Sponsored by

Defense Advanced Research Projects Agency (DoD)
DARPA Order No. 4540
Monitored by Naval Research Laboratory
Under Contract No. N00014-82-C-2466

UNCLASSIFIED
SECURITY CLASSIFICATION OF THIS PAGE

AD-A138693

REPORT DOCUMENTATION PAGE

1a. REPORT SECURITY CLASSIFICATION Unclassified	1b. RESTRICTIVE MARKINGS
2a. SECURITY CLASSIFICATION AUTHORITY	3. DISTRIBUTION/AVAILABILITY OF REPORT Approved for public release; distribution unlimited.
2b. DECLASSIFICATION/DOWNGRADING SCHEDULE	
4. PERFORMING ORGANIZATION REPORT NUMBER(S) SC5340.4SA	5. MONITORING ORGANIZATION REPORT NUMBER(S)
6a. NAME OF PERFORMING ORGANIZATION Rockwell International Science Center 6b. OFFICE SYMBOL (If applicable)	7a. NAME OF MONITORING ORGANIZATION
6c. ADDRESS (City, State and ZIP Code) 1049 Camino Dos Rios Thousand Oaks, California 91360	7b. ADDRESS (City, State and ZIP Code)
8a. NAME OF FUNDING/SPONSORING ORGANIZATION Naval Research Laboratory 8b. OFFICE SYMBOL (If applicable)	9. PROCUREMENT INSTRUMENT IDENTIFICATION NUMBER Contract No. N00014-82-C-2466
8c. ADDRESS (City, State and ZIP Code) 4555 Overlook Avenue S.W. Washington, D.C. 20375	10 SOURCE OF FUNDING NOS. PROGRAM ELEMENT NO.: DARPA ORDER NO. 4540 PROJECT NO. TASK NO. WORK UNIT NO.
11. TITLE (Include Security Classification) (U) FERROELECTRIC TUNGSTEN BRONZE BULK CRYSTALS AND EPITAXIAL THIN FILMS FOR ELECTRO-OPTIC DEVICE APPLICATIONS	
12. PERSONAL AUTHOR(S) Neurgaonkar, Ratnakar R., Cross, L.E.	
13a. TYPE OF REPORT Semi-Annual Tech Rpt. #2 13b. TIME COVERED FROM 04/01/83 TO 09/30/83	14. DATE OF REPORT (Yr., Mo., Day) FEBRUARY 1984 15. PAGE COUNT 63
16. SUPPLEMENTARY NOTATION Total pages 12th [illegible]	
17 COSATI CODES FIELD / GROUP / SUB. GR.	18. SUBJECT TERMS (Continue on reverse if necessary and identify by block number) SBN, PBN, Czochralski, LPE Growth, Tungsten Bronze, Flux Systems, Electro-optic Coefficients, Striations, Birefringence.

19. ABSTRACT (Continue on reverse if necessary and identify by block number)

SBN:50 and SBN:60 crystals have now been grown with improved optical quality using the Czochralski technique with automatic diameter control. The liquid phase epitaxial (LPE) growth of SBN:50 on SBN substrates has also been successfully demonstrated, with particularly good results for (100) and (110) film orientations. Electro-optic measurements on SBN:60 single crystals have shown a high value for r_{51} of 80×10^{-12} m/v, nearly a factor of 2 greater than for SBN:75.

The tungsten bronze system $Pb_{1-x}Ba_xNb_2O_6$ (PBN) has shown enhanced piezoelectric, dielectric and optical properties near the morphotropic boundary at x = 0.37. Substantial data on the physical properties of PBN single crystals is presented as a function of composition. Work on an appropriate flux system for LPE growth of PBN is in progress, with particular focus on the system $Pb_2V_2O_7$ - PBN:60.

Systematic work on the tungsten bronze systems $Ba_2NaNb_5O_{15}$ - $Sr_2NaNb_5O_{15}$ (BNN-SNN) and $Pb_2KNb_5O_{15}$ - $Ba_2NaNb_5O_{15}$ (PKN-BNN) has been undertaken, with both systems showing morphotropic boundary conditions with enhanced dielectric properties. Both systems look promising for future electro-optic development.

20. DISTRIBUTION/AVAILABILITY OF ABSTRACT UNCLASSIFIED/UNLIMITED ☒ SAME AS RPT. ☐ DTIC USERS ☐	21. ASSTRACT SECURITY CLASSIFICATION Unclassified
22a. NAME OF RESPONSIBLE INDIVIDUAL Neurgaonkar, Ratnaker R.	22b. TELEPHONE NUMBER (Include Area Code) (805) 498-4545 22c. OFFICE SYMBOL

DD FORM 1473, 83 APR EDITION OF 1 JAN 73 IS OBSOLETE.

UNCLASSIFIED
SECURITY CLASSIFICATION OF THIS PAGE

TABLE OF CONTENTS

TABLE OF CONTENTS

LIST OF FIGURES

LIST OF TABLES

1.0 SUMMARY AND PROGRESS

The tungsten bronze structural family offers a large number of crystals for electro-optic and nonlinear optical applications. However, the current work has mainly focused on the development of optical quality crystals/films for the bronze $Sr_{1-x}Ba_xNb_2O_6$ (SBN) system. Considerable progress has been recently made in different areas including bulk crystal growth, film growth and electro-optic characterization, as well as in phenomenological modeling work. An overall view of the important activities of this project and their interrelationship is shown in Fig. 1.

Several SBN:60 single crystals have been grown by the Czochralski technique, and the quality of the crystals seems to be much improved by controlling the pulling conditions with the use of an automatic diameter control (ADC) system. It has been shown that the striations depend not only on the quality of the starting materials, but also on how the ADC system is used when pulling these crystals. The SBN:60 and SBN:50 single crystals have now been grown as large as 1-2 cm in diameter and about 4-5 cm in length. The primary use of the SBN:50 single crystals is as substrate material for the proposed liquid phase epitaxial (LPE) growth work.

We have successfully demonstrated the use of the LPE growth technique to develop thin films of $Sr_{0.5}Ba_{0.5}Nb_2O_6$ on SBN substrates. Although the rate of crystallization along the (001) direction is much faster as compared to other orientations, growth is more difficult on (001)-plate SBN substrates due to a slight mismatch in lattice constants. On the other hand, growth along the (110) and (100) directions has been successful and the quality of the films is much better. It is important to note that the electro-optic r_{33} coefficient is also largest along the (100) direction.

Recent work on SBN:60 single crystals has shown a value for the electro-optic coefficient, r_{51}, of 80×10^{-12} m/V, a value significantly greater than for SBN:75 (42×10^{-12} m/V) which possesses an optimum value for

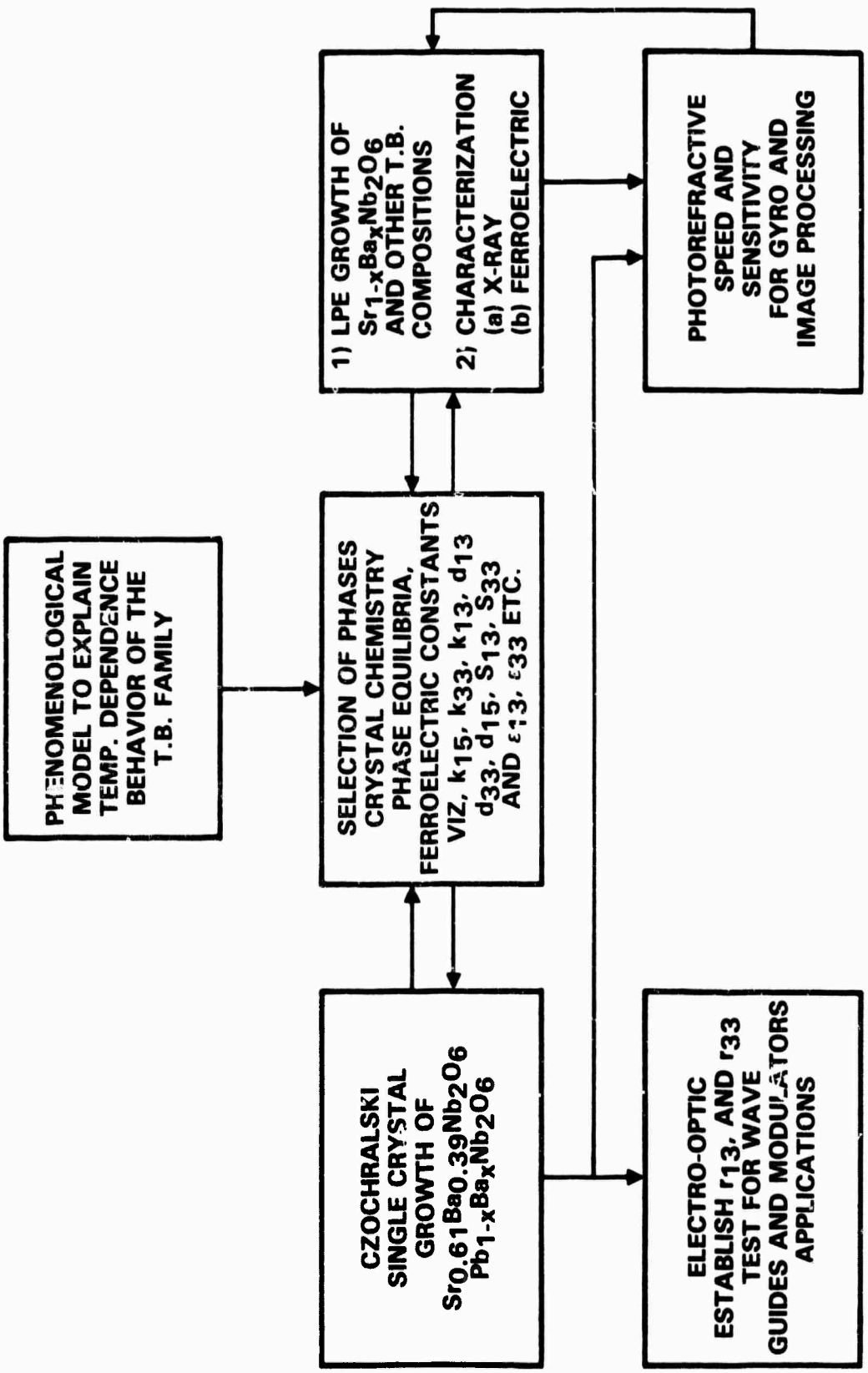

Fig. 1 Flow chart of activities.

r_{33}. This indicates that r_{51} is compositionally dependent on the concentration of Ba^{2+}, but in a manner opposite to the behavior of r_{33}. This could be a significant result for the potential application of SBN crystals in optical switching and spatial light modulator devices.

Another important bronze system, $Pb_{1-x}Ba_xNb_2O_6$ (PBN), has been selected for study in this work. This system exhibits a morphotropic phase boundary at x = 0.37, and compositions near this point show exceptionally high electro-optic and dielectric properties. Since bulk single crystal growth of PBN is difficult due to volatilization of Pb^{2+}, the LPE technique will be used to develop this material for optical studies. At present, the flux system $Pb_2V_2O_7$-$Pb_{0.6}Ba_{0.4}Nb_2O_6$ is being developed for thin film growth.

Several of the more interesting tungsten bronze systems show morphotropic phase boundaries which depend primarily on composition rather than on temperature. Ceramic compositions adjacent to these boundaries show enhanced electro-optic, pyroelectric, dielectric and electromechanical factors because of the proximity in energy to the alternate ferroeletric structure. Systematic work is in progress on the tungsten bronze systems $Ba_2NaNb_5O_{15}$-$Sr_2NaNb_5O_{15}$ (BNN-SNN) and $Pb_2KNb_5O_{15}$-$Ba_2NaNb_5O_{15}$ (PKN-BNN) to establish their dielectric, electro-optic and pyroelectric properties. Once this task has been completed, a few compositions from each system will be further developed for optical device applications.

2.0 DEVELOPMENT OF TUNGSTEN BRONZE MATERIALS

2.1 Materials Growth Techniques

Since most of the bronze compositions grown in our laboratory are based on solid solution systems, it is important that suitable growth techniques be developed to produce crystals free of optical defects such as striations, scattering centers and twinning. Striations and other defects are typical problems common to solid solution crystals, and it is often difficult to suppress them completely. However, these problems can effectively be reduced such that the crystals can be useful for optical device studies. This task is difficult; hence, the selection of appropriate growth techniques is critical in the present work. At present, three different techniques have been chosen to develop SBN and other bronze crystals. They are as follows:

1. Bulk Single Crystals: Czochralski technique.
2. Thin Films: Liquid phase epitaxy (LPE).
3. Strip Crystals: Edge defined film-fed technique.

The first two techniques are well established in our current work, and bulk crystals and films of SBN compositions have already been grown. In the present report, the growth of striation-free SBN crystals and films is discussed with the associated growth problems.

2.2 Growth Procedure

Nb_2O_5, $SrCO_3$ and $BaCO_3$ fine powders have been used as starting materials and weighed out in the desired proportions, as summarized in Table 1. The batch mixture is ball-milled in acetone for 20-30 h, and then poured into a large drying dish. The dried powder is placed in a platinum reaction dish and calcined at 1000°C for 10-15 h to eliminate carbonates and any possible carbon from the pyrolytic breakdown of residual acetone. The calcined powder is then ball-milled again and refired in an oxygen flow of 2 cfh at 1400°C for

Table 1

Materials for Bulk Single Crystal Growth Work

Crystal Composition	Starting Materials**		Remarks
SBN:60	a. $SrCO_3$	135.08 gms	* Congruent melting composition.
	b. $BaCO_3$	115.45 gms	* Large crystals can be produced approximately 1" in diameter.
	c. Nb_2O_5	398.73 gms	* Used as host crystal, as well as substrate material for LPE work.
	Total wt	649.26 gms	* Exhibits high electro-optic and pyroelectric coefficients.
	Total wt used for growth	450.0 gms	* Melts at 1510°C and no spattering observed.
SBN:50*	a. $SrCO_3$	92.26 gms	* Slightly off congruent melting composition.
	b. $BaCO_3$	123.34 gms	* Large crystals are available.
	c. Nb_2O_5	332.27 gms	* Used as substrate material for LPE work.
	Total wt used for growth	547.87 gms	* Modified crystals exhibit excellent pyroelectric properties.
			* Melts at 1520°C
SBN:75	a. $SrCO_3$	166.05 gms	* Exhibits highest electro-optic and pyroelectric coefficients.
	b. $BaCO_3$	73.98 gms	* Used as substrate, as well as host material.
	c. Nb_2O_5	399.00 gms	* Slightly off congruent melting composition.
	Total wt	639.03 gms	* Melts at 1500°C.
	Total wt used for growth	450.0 gms	

* La^{3+} doped SBN:50 crystals have also been grown.
** Chemical analysis of each starting material is given in an earlier report.

about 4-6 h. Phase checks and x-ray lattice constant measurements are made for each batch to ensure the use of a phase-pure bronze composition for crystal growth. A thick-walled platinum crucible of 2 x 2 in. in dimension is used for this growth, and this container holds roughly 450 g of melt composition.

2.3 Growth of Tungsten Bronze $Sr_{1-x}Ba_xNb_2O_6$ Crystals

Table 2 gives a brief summary of our crystal growth effort on the tungsten bronze ferroelectric $Sr_{1-x}Ba_xNb_2O_6$, x = 0.40 and 0.50, single crystals grown by the Czochralski technique. Since the growth of the SBN:75 composition was only recently initiated, Table 2 does not include growth data on this crystal. However, the importance of this composition is discussed in this section. Table 3 summarizes the ferroelectric, electro-optic and pyroelectric characteristics of SBN:60, SBN:50 and SBN:75. Using these crystals, one may formulate several device applications; hence, their growth is very important. The results of these investigations are as follows:

SBN:50

This composition has mainly been selected in the present study to be used as substrate material for the LPE growth of bronze family compositions. The growth of this composition has already been reported by several researchers.[1-5]. Growth is rather difficult as compared to the congruent melting composition, SBN:60, due to cracking of crystals when cycling through the paraelectric/ferroelectric phase transition temperature; hence, the size of these crystals has been confined to 1 cm or less. We are presently studying the cracking problems for these crystals and have eliminated them to a large

extent, enabling us to grow crystals ~ 1-1.5 cm in diameter. Figure 2 shows a typical 1.5 cm SBN:50 crystal pulled along the (001) direction. La^{3+}-modified SBN:50 single crystals have also been developed and they show an exceptionally high pyroelectric response, making them potentially useful for uncooled infrared detector applications. Plans have been made to pull these crystals using the ADC system so that one may better control the diameter, thereby further reducing crystal cracking.

Table 2
Growth of SBN Single Crystals

To NRL	Boule No.	Date Grown	Comp. Sr/Ba	Boule wt, gm	Boule Size, cm	Dopant wt%	Dip °C	Pull Rate	Rotation rpm	Remarks, Observations
	148	04/22/83	50/50*	35	2.0 x 2.5	--	1490	~ 5	10	Striae-free regions; some cracks
	149	04/26/83	60/40	44	1.8 x 3.0	--	1490	~ 5	10	Uncracked, stria-free regions
	150	04/29/83	60/40	15	1.2 x 2.5	--	1492	10-12	10	Uncracked
	151	05/03/83	50/50*	28	1.5 x 2.7	0.29 wt% La_2O_3	1490	6	0-5	Cracks on one side; annealing in O_2 does not change boule color
	152	05/16/83	50/50	37	1.8 x 2.7	11	1490	5	11	Several cracks - large twins
	153	05/23/83	60/40	16	1.0 x 2.5	--	1490	~ 5	12	Uncracked
*	154	06/10/83	60/40	24	1.4 x 4.0	--	1491	10-14	10	Good widening cone; striae-free regions, uncracked
*	155	06/17/83	60/40	38	1.5 x 4.0	--	1492	9-12	~ 15	~ 50% striae-free - last boule from charge. Large bubble bottom 1/3; cracks below bubble
	156	07/25/83	50/50*	35	1.7 2.5	0.29 wt% La_2O_3	1490	~ 6	~ 6	Cracked
	157	08/25/83	60/40	44	1.5 x 4.0	--	~ 1490	8-12	5-10	First growth from new charge; uncracked
	158	08/30/83	50/50*	38	1.6 x 3.0	.58 wt% La_2O_3	~ 1490	~ 10	5	Cracks, but usable samples
*	159	09/02/83	60/40	40	1.5 x 4.5	--	~ 1490	~ 8	~ 10	Minor coiling, uncracked
	160	09/06/83	60/40	49	1.9 x 4.3	--	~ 1490	5-12	~ 7	3 cm of very straight growth, uncracked except near one surface twin
	161	09/13/83	60/40	32	1.4 x 3.5	--	~ 1490	10-12	~ 7	ADC not used; uncracked
*	162	09/16/83	60/40	52	1.7 x 4.0	--	~ 1490	10	~ 8	Minor coiling, uncracked
	163	09/20/83	60/40	42	1.4 x 5.0	--	1492	10-12	~ 8	Uncracked
*	164	10/18/83	60/40	40	1.5 x 4.3	--	1492	~ 10	3-8	1 inch long straight portion, uncracked
	165	10/21/83	60/40	44	1.6 x 4.0	--	1492	6-12	~ 6	Slightly off c-axis, uncracked
	166	10/26/83	60/40	31	1.5 x 3.0	0.4 wt% Fe_2O_3	1492	10	6	Stress in center; one basal crack and one vertical crack in lower 2.0 cm. Anneals to clear green color

Oxygen atmosphere was used for all crystals.

SC83-22629

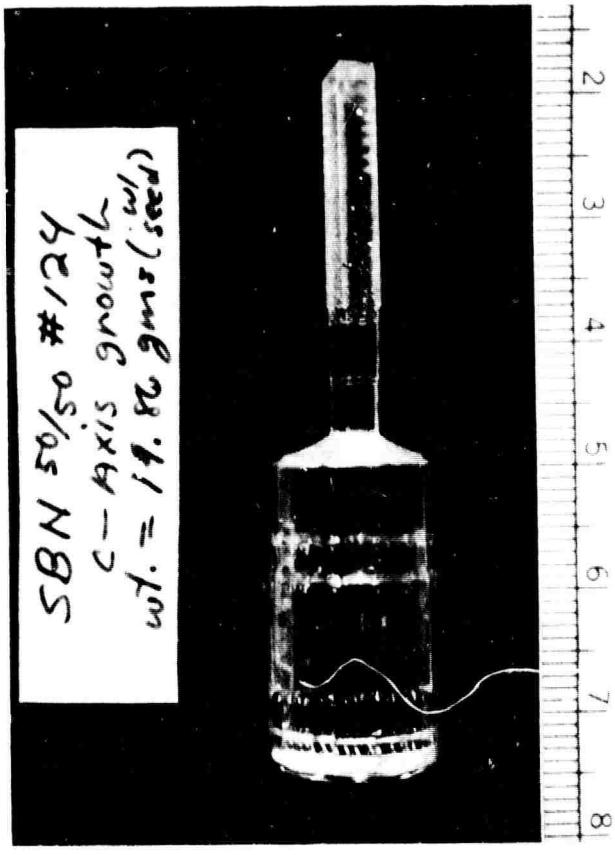

Fig. 2 SBN:50 single crystal grown along the (001) direction.

Table 3

Ferroelectric, Electro-Optic and Pyroelectric Properties of the SBN System

Property	SBN:75	SBN:60	SBN:50*
Symmetry	4 mm	4 mm	4 mm
Lattice Constant	a = 12.457Å c = 3.928Å	a = 12.475Å c = 3.940Å	a = 12.482Å c = 3.952Å
T_c (°C)	56	72	125
Dielectric Constant at R.T.	ε_{33} = 3400	ε_{33} = 600	ε_{33} = 500
Electro-Optic Coefficient x 10^{-12} m/V	r_{33} = 1400	r_{33} = 420	r_{33} = 120
Pyroelectric Coefficient C/cm^2-K	P = 2800	P = 880	P = 680*
Piezoelectric Coefficient x 10^{-12} C/N	d_{33} = -- d_{15} = --	d_{33} = 130 d_{15} = 31	d_{33} = 110 d_{15} = 28
Electromechanical Coupling Constant	K_{33} = -- K_{15} = --	K_{33} = 0.45 K_{15} = 0.24	K_{33} = -- K_{15} = --

* Pyroelectric coefficient for SBN:50 (La^{3+}) = 1170

SBN:75

This composition exhibits the largest electro-optic (r_{33} = 1400 x 10^{-12} m/V) and pyroelectric coefficients of any well-behaved oxide material.[6,7] These features make this crystal potentially attractive for future electro-optic, pyroelectric, photorefractive and millimeter wave applications. If and when this crystal composition becomes available in optical quality, it will create a significant scientific impact in electro-optic and other device research areas. The growth of this composition has recently been initiated, and small crystals will be grown to identify problems associated

with Czochralski growth. Based on this work, necessary changes in growth procedures will be made to obtain good optical quality SBN:75 crystals.

SBN:60

As discussed in a previous report,[8] the single crystal growth technique of SBN:60 has been modified in order to improve the crystal quality and thereby enhance its use for optical studies. Since SBN:60 is reported to be the only congruent melting composition in $SrNb_2O_6$-$BaNb_2O_6$ system,[9] the current effort has mainly concentrated on this composition. It is now well established that there are several factors that influence the quality and size of bronze crystals. Hence, it is important that the necessary modifications be made in our growth procedure from time to time. The changes made are as follows:

1. Use of higher purity starting materials to eliminate striations caused by impurity ions, i.e., Fe^{3+}, Ca^{2+} and Na^{+}.
2. Eliminated the use of iridium crucible: no iridium contamination.
3. Established pulling and rotation rates for SBN:60 crystals.
4. Effectively utilized the ADC system to minimize temperature instability during growth.

Except for the last parameter, the necessary changes have been made in our earlier growths, as discussed in detail in our last report. During the last six months, considerable progress has been made in understanding temperature fluctuations and the application of the ADC system during growth. The results of this work are discussed in the following section.

2.4 Growth of SBN:60 Crystals With ADC System

The need for automatic diameter control (ADC) in growing SBN:60 single crystals arises mainly from the poor tnermal conductivity of the mate-

rial, which causes great difficulty in maintaining a fixed crystal diameter by set-point programming of the furnace power. It has been noticed that small changes on the order of ± 1° to 2° in the thermal environment near the growing interface tend to continually upset the steady state heat flow through the crystal, either increasing it to cause crystal widening or decreasing it to cause crystal narrowing. Uniform crystal diameter implies unchanging melt temperature near the interface, a necessary and important ingredient for producing homogeneous, striae-free crystals, and this has been recently achieved to a large extent in SBN crystals. As shown in Fig. 3, the striae pattern of crystals sectioned and polished parallel to the growth axis (001) clearly show that the growth under rapidly changing thermal conditions (left) contains strong striae, then a transition zone occurs (center) as the crystal begins to achieve constant diameter. In this section, striae tend to be weak. ADC is engaged during at this point and, as growth continues, the system settles down to constant diameter growth with striae absent, or nearly so (extreme right). This is a significant accomplishment in this program, and it has successfully shown that the ADC system can be effectivly used to maintain uniform crystal diameter and thereby reduce or eliminate striations. Figure 4 shows a typical 1.5 cm diameter, 6-7 cm long SBN crystal grown along the (001) direction using the ADC system. This is the first time such long and uniform diameter SBN:60 single crystals have been grown in this program.

A crucible-weighing ADC system has been installed for this task, since the technology is well established and good equipment is commercially available. The ADC system has been modified in the current arrangement, with some furnace redesign necessary and electronically matched to the growth furnace thermal time constant to achieve the smoothest possible changes in furnace power to hold the growth interface conditions as steady as possible. This has been accomplished over a period of many experiments. It has been observed that the present system gives its best performance (achieving ± 1°C) when crystals are grown in large sizes of ~ 1 cm or larger in diameter. Below this limit, the sensitivity of this system was found to be inadequate.

SC83-24485

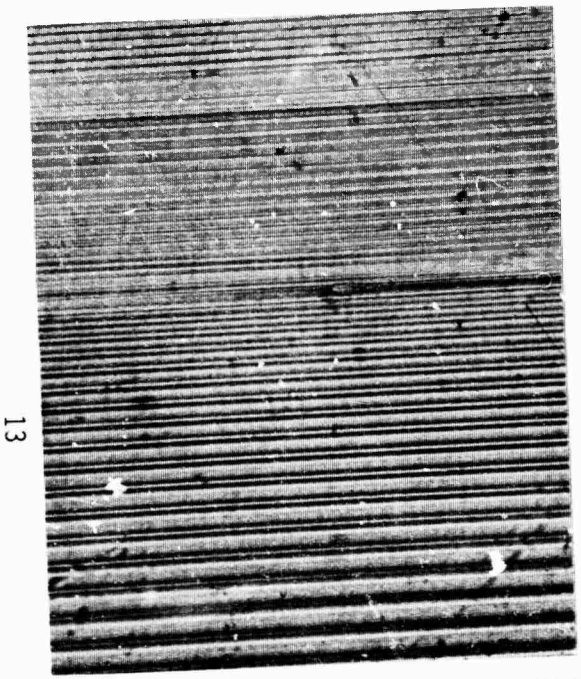

SBN:60 CRYSTAL GROWTH WITHOUT ADC SYSTEM

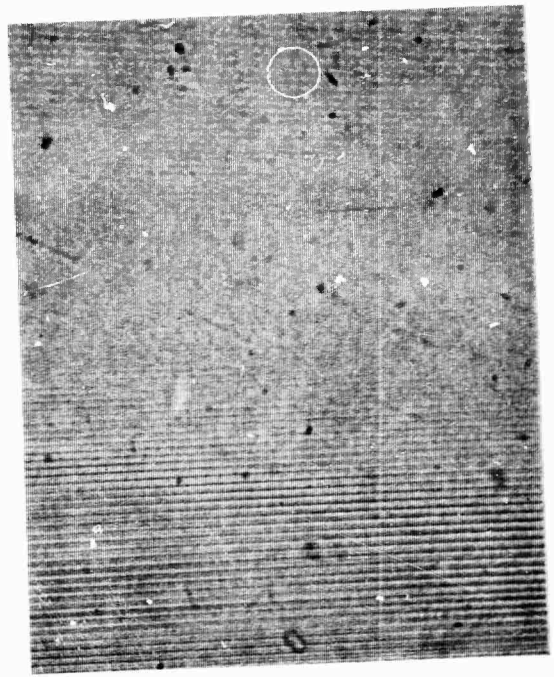

SBN:60 CRYSTAL GROWTH WITH ADC SYSTEM (UNSTABLE CONDITIONS)

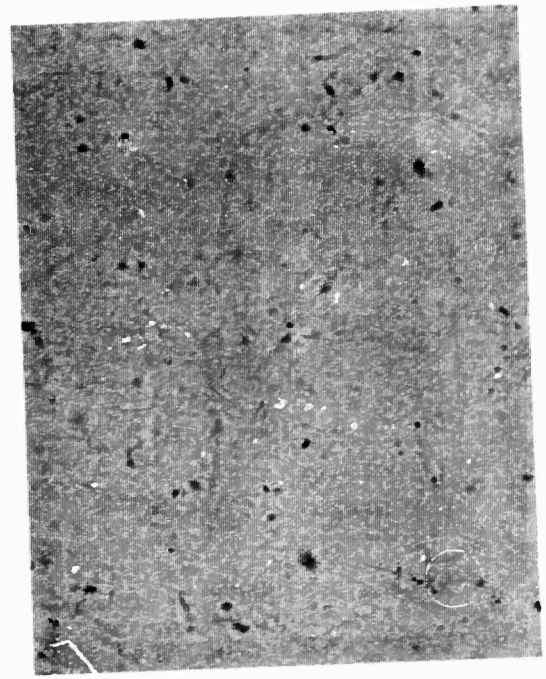

SBN:60 CRYSTAL GROWTH WITH ADC SYSTEM AFTER ESTABLISH CONDITIONS

Fig. 3 Growth of striation-free ferroelectric SBN:60 single crystals.

SC84-25778

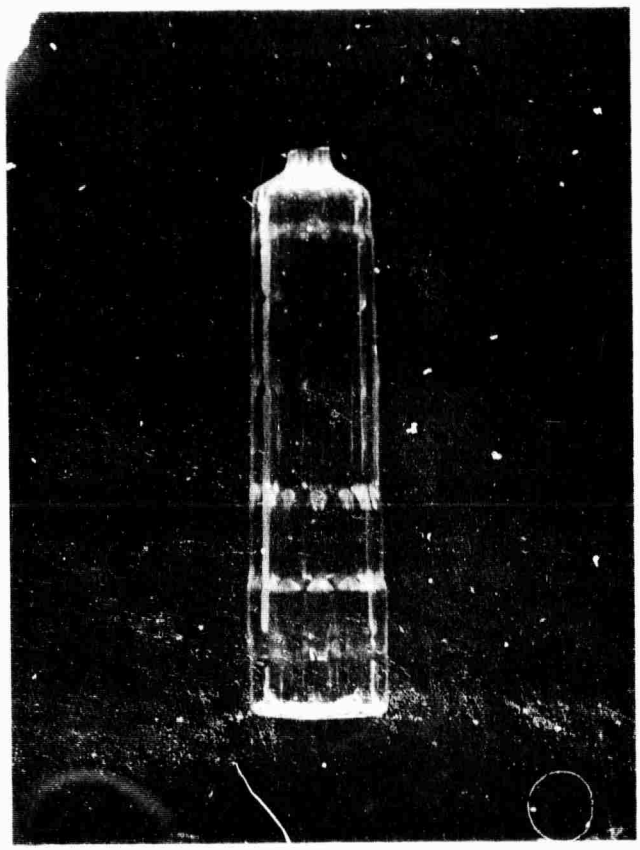

Fig. 4 SBN:60 crystal grown along the [001] direction using the ADC system.

Further improvements are underway to control interface conditions, i.e., control temperature fluctuations to below ± 1/2°C to produce even better diameter control and hence more homogeneous crystals. We also plan to install a crystal weighing ADC system which may be combined with pull rate diameter control for improved control of the interface shape and heat flow. An automatic variable cross-section control will allow completely automatic widening and tailing of crystals. Computer programming and control of all these functions should lead to completely automatic growth of crystals from "seed on" to decant.

In summary, the quality of SBN:60 single crystals has been dramatically improved, and has created new interest and applications for this crystal. What we plan to accomplish during the next six months is to show that the growth process is reproducible, at least for small crystals, and the quality can be effectively controlled. For further improvement and reproducibility, the following changes are planned:

- Improve centering of the radial gradient in the melt to further reduce or eliminate striations and coring effects.

- Study the effects of the after-heater furnace on the radial and axial gradients and the optimum pull rate.

- Reduce melt impurity level by selecting the highest quality starting materials, specifically Nb_2O_5.

- The role of pull rate and rotation will be reinvestigated with respect to the current upgraded growth process.

3.0 LIQUID PHASE EPITAXIAL GROWTH OF BRONZE COMPOSITIONS

3.1 Introduction

The purpose of the liquid phase epitaxial (LPE) growth work is to develop optical quality ferrolectric tungsten bronze family compositions that possess high electro-optic, nonlinear optical, and piezoelectric properties with a moderately low dielectric constant. We recently demonstrated the successful growth of striation-free SBN:60 single crystals by the Czochralski technique, and crystals as large as 1-2 cm in diameter have been produced. However, we believe that this technique may not be adequate for other bronze compositions such as $Ba_2KNb_5O_{15}$ (incongruent melting), $Pb_{1-x}Ba_xNb_2O_6$, and $Pb_2KNb_5O_{15}$ (volatilization of Pb^{2+}). In these instances, it is expected that the LPE technique should play an important role in developing a wider variety of ferroelectric bronze compositions for optical applications. Furthermore, the ability of LPE to obtain a wide variety of films in a relatively short time, compared with the time required to achieve suitable quality single crystals, will enable us to greatly expand our knowledge of obtainable properties in this class of families. Since large crystals of the bronze compositions $Sr_{1-x}Ba_xNb_2O_6$, x = 0.40 and 0.50, and BSKNN (ONR and NVL) are now available from our current work, and the lattice mismatch between the selected crystals and proposed compositions is minimal, we do not anticipate any major problem in developing heteroepitaxial growth for several of these bronze compositions. Although several compositions have been identified as potential candidates for this work, the current research has been restricted to a few ferroelectric systems, e.g., $Sr_{1-x}Ba_xNb_2O_6$ and $Pb_{1-x}Ba_xNb_2O_6$. In the latter system, both the orthorhombic and tetragonal tungsten bronze structures exist, which makes this system potentially important for optical studies. The experimental work on both systems is in progress and the initial results of these investigations are discussed in the following sections.

3.2 Summary on LPE Growth Experiments

As discussed in an earlier report, the LPE growth technique has been successfully developed for the ferroelectric $Sr_{0.5}Ba_{0.5}Nb_2O_6$ composition using BaV_2O_6 solvent and $Sr_{0.6}Ba_{0.4}Nb_2O_6$ substrates. The liquidus temperature and compositional boundary conditions for this composition were determined by establishing the phase diagram for the pseudo-binary system BaV_2O_6-$Sr_{0.5}Ba_{0.5}Nb_2O_6$. Based on this work, a mixture containing 65 mole% BaV_2O_6 and 35 mole% $Sr_{0.5}Ba_{0.5}Nb_2O_6$ was found to be suitable because: 1) the composition of the resulting phase is close to $Sr_{0.4}Ba_{0.6}Nb_2O_6$, and 2) the composition melts at a relatively low temperature (1000°C). Detailed information on ternary and binary systems is provided in our earlier report.[8]

Initially, (001) oriented $Sr_{0.6}Ba_{0.4}Nb_2O_6$ substrates were used, and the LPE process was established for this composition. Films as thick as 5-35 μm were easily grown at about 1000°C. After cleaning the films in diluted HCl or HNO_3 acids, it was found that the films grown from the V^{5+}-containing flux were dark amber to yellow in color, indicating possible inclusion of V^{5+}. The results of x-ray diffraction and other ferroelectric measurements ruled out such a possibility due to a strong tetrahedral preference of the V^{5+} cation. The surfaces were smooth and clean, but showed a tendency towards cracking after film removal from the growth furnace. This is believed to be due to a slight mismatch between the film/substrate lattice constant, c. As can be seen from Table 4, the mismatch for the other orientations such as (100) is much less, and we found growth along the (100) and (110) directions to be much more successful. Hence, substrates oriented along (100) and (110) are being used for the present study. Once LPE growth is well established for these orientations, growth on the (001) orientation will be continued. It is interesting to note that the optimum electro-optic coefficient, r_{33}, is also observed[6] along the (100) direction of tetragonal tungsten bronze crystals, and this could be a beneficial orientation for future electro-optic characterization. However, for optical waveguides, one may need other orientations such as (001).

Table 4

Structural Data For the SBN Substrate/Film

Material		X-Ray Diffraction Data (8,0,0)		(10,0,0)		(12,0,0)	
		$CuK\alpha_1$	$CuK\alpha_2$	$CuK\alpha_1$	$CuK\alpha_2$	$CuK\alpha_1$	$CuK\alpha_2$
Substrate, SBN:60	2θ	59.241	59.413	76.321	76.546	95.703	96.023
	I/I_o	60.1	21.1	100.1	50.1	96.1	50.1
	a Å	12.475Å		12.478Å		12.481Å	
Film, SBN:50*	2θ	59.000	59.182	76.003	76.223	95.251	95.571
	I/I_o	100.1	60.1	100.1	60.1	100.1	65.1
	a Å	12.501	12.503	12.500	12.5001	12.498	12.496

* Composition of film is slightly changed as compared to melt composition. Tentative composition is $Sr_{0.4}Ba_{0.6}Nb_2O_6$.

Although the crystallization rate for the SBN:60 composition is much faster along the (001) direction compared to the (100) and (110) orientations, the latter films are of better quality and films as thick as 10-25 μm have been easily grown. At present, efforts are being made to establish the influence of temperature variations and growth time on film thickness and compositional fluctuation. Although the growth of SBN films has been shown to be successful, all of the experimental factors have not yet fully been identified from the current work regarding the growth rate and tolerance factors for lattice match/mismatch for each orientation. Future work includes these tasks and also includes plans to grow other bronze compositions based on the $Pb_{1-x}Ba_xNb_2O_6$ system.

3.3 Characterization of Films

Before films can be used for any device application study, it is important that their quality and ferroelectric properties be established using x-ray diffraction and ferroelectric measurement techniques. During the last six months, considerable progress has been made in these areas. The details of

the x-ray diffraction measurements and poling techniques are discussed in the following sections.

3.3.1 Structural Characterization

The crystallinity, composition and lattice constant, a, have been established by x-ray diffraction measurements. Typical intensity vs epilayer thickness plots are given for the reflections (800), (10,0,0) and (12,0,0) in Fig. 5. Two peaks corresponding to $CuK\alpha_1$ and $K\alpha_2$ represent the SBN:60 substrate, while the nominal SBN:50 epilayer position is denoted by $CuK\alpha'_1$ and $K\alpha'_2$. The intensity of the epilayer reflection is slightly stronger than that of the substrate, indicating a high degree of crystallinity and successful deposition of the SBN layer on the SBN:60 substrate.

For determination of the composition of the thin films, the lattice constant a for film/substrate was carefully evaluated using Si as the internal standard. A small amount of Si was placed with the film on a glass substrate for the x-ray measurements, and as shown in Fig. 5, three reflections, namely (8,0,0), (10,0,0) and (12,0,0), were carefully recorded. The resolution for film and substrate peaks was excellent and reflections were accurately measured by scanning at 1/8°/min. The observed 2θ for each reflection are given in Table 4. Using these values, the lattice constant, a, for film and substrate are 12.500Å and 12.478Å, respectively. By comparing the film a value with the lattice constant for the $Sr_{1-x}Ba_xNb_2O_6$ system, it appears that the film composition is close to $Sr_{0.40}Ba_{0.60}Nb_2O_6$. The results clearly indicate that the film composition is slightly changed from the melt with an increased Ba^{2+} concentration.

Since the films are grown from BaV_2O_6 solvent, it is important that the Ba:Sr ratio in the solvent be controlled. Based on the work by Lenzo et al,[6] the composition $Sr_{0.75}Ba_{0.25}Nb_2O_6$ exhibits the highest electro-optic and pyroelectric coefficients; hence, it is important in the present work to develop films close to this composition. As shown in the ternary diagram, BaV_2O_6-$SrNb_2O_6$-$BaNb_2O_6$ (Fig. 6), the $Sr_{0.75}Ba_{0.25}Nb_2O_6$ phase is located at the

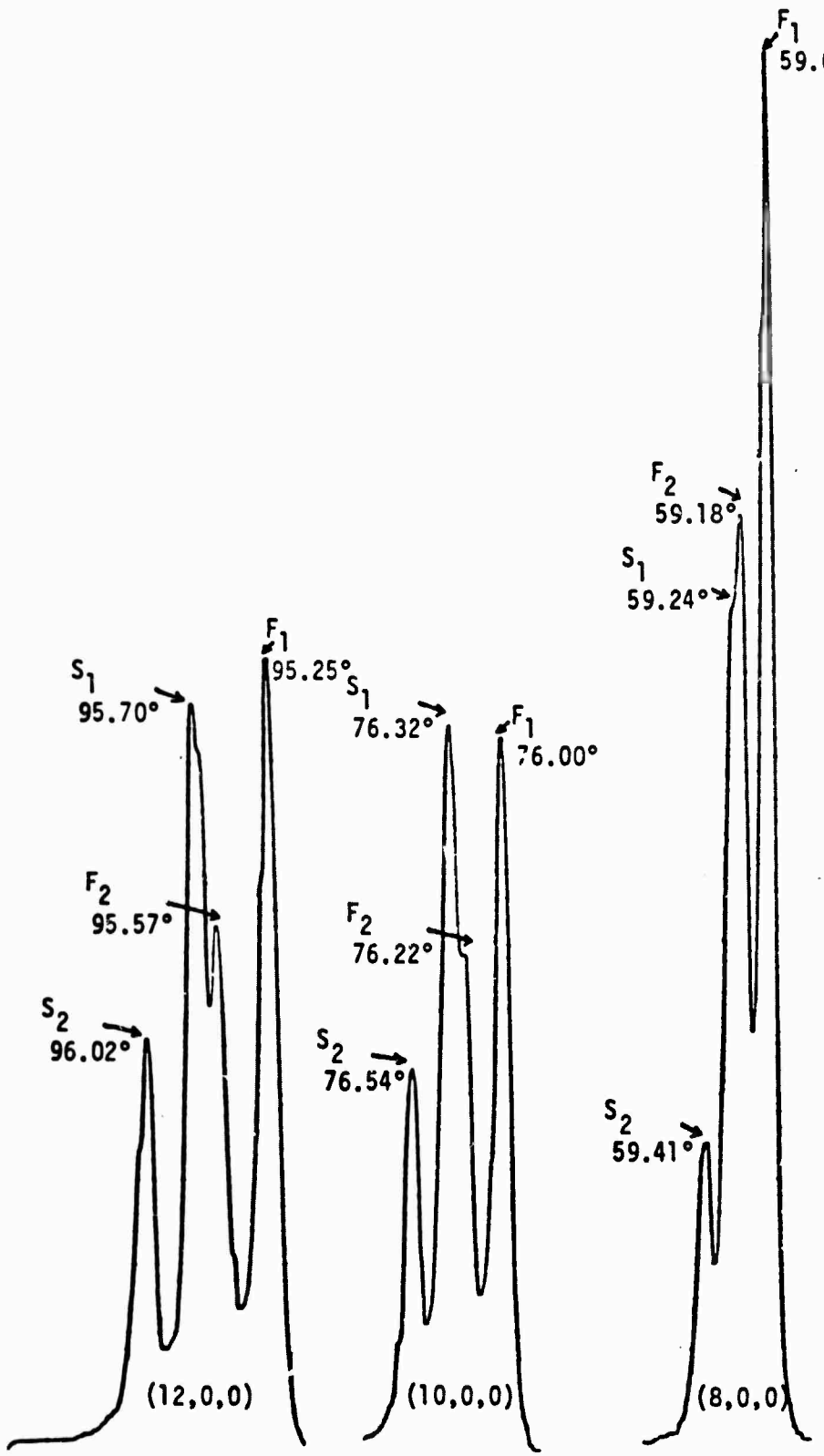

Fig. 5 X-ray diffraction peaks taken for substrate/film.

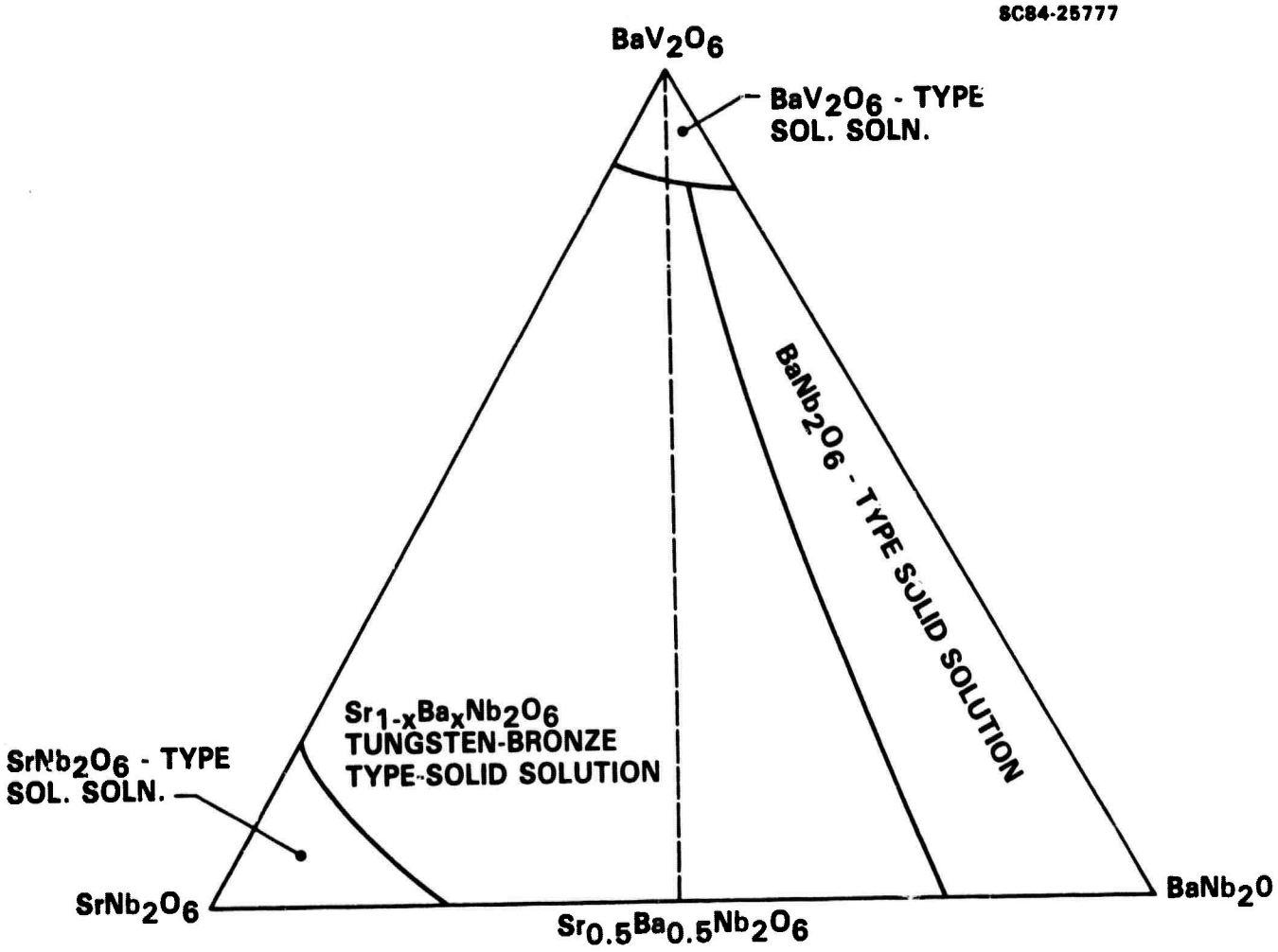

Fig. 6 The system BaV_2O_6-$BaNb_2O_6$-$SrNb_2O_6$ in air at 1200°C.

Sr^{2+}-rich end, and this suggests that for future LPE work it is desirable that the films be grown from a Sr^{2+}-rich solvent. Work is in progress to develop such compositions by controlling the melt in the following two ways:

1. $Ba_{1-x}Sr_xV_2O_6$-$Sr_{0.75}Ba_{0.25}Nb_2O_6$, or

2. SrV_2O_6-$Sr_{1-x}Ba_xNb_2O_6$

The results of x-ray measurements on both these systems indicate the existence of the tetragonal tungsten bronze phase. However, the precise composition is not yet fully established. Further x-ray work is underway to establish the lattice constants and allow us to modify the melt composition accordingly.

3.3.2 Poling

To obtain optimum data concerning piezoelectric, pyroelectric, electro-optic, or even nonlinear optical properties of ferroelectric crystals, it is necessary to work with single domain pieces. Therefore, it is important in this work to prepare single domain SBN films for evaluation of their optical properties. Based on dielectric temperature dependence measurements on SBN:60 single crystals, the ferroelectric transition temperature (T_c) occurs at 72°C; this information is absolutely required. The procedure for poling used here consisted of heating the grown SBN single crystal to about 5°C below T_c, with a dc field between 1-6 KV/cm along the c-axis of the sample for a time corresponding to 1 h per cm length. The electrode materials used were either gold or platinum. It has been shown that an approximately 5.0 kV/cm field is needed to obtain single domain SBN:60 single crystals. However, poling becomes more difficult when crystals are used with different orientations. In tetragonal SBN crystals, the [001] direction is polar, and poling has been accomplished along this direction. Hence, this orientation has to be maintained, at least in the plane, in order to pole crystals with other orientations.

In the case of (100) and (110) plates, the [001] axis lies in the plane, and the poling field must be oriented along the length of the sample (Fig. 7b). Electrodes were deposited on the ends of the samples with some overlap (typically 1 mm) onto the major faces. Surface conductivity is a major problem in this configuration because of the high poling voltages required, and hence, good surface preparation and cleanliness is essential. These samples were successfully poled using the same procedure outlined above, but at a slightly higher field (7.5-8.0 kV/cm).

The poling of (100) and (110) plates is a significant accomplishment in this work. The next task will be to apply this technique to (100) oriented substrates with epilayer films having a Curie point much higher than that of the substrate. Although the most effective (and nondestructive) poling procedure under these circumstances is not presently known, it is anticipated that poling will be achieved by raising the temperature to the Curie point of the film, and then slowly cooling while maintaining a high voltage dc field. This procedure should result in a simultaneously poled film/substrate. Initial research into this probem is now in progress.

3.4 The Tungsten Bronze $Pb_{1-x}Ba_xNb_2O_6$

The ferroelectric $Pb_{1-x}Ba_xNb_2O_6$ system is considered to be promising for use in various device applications, e.g., pyroelectric, electro-optic piezoelectric, etc. It has also been shown thermodynamically using Landau: Ginsburg:Devenshire (LGD) phenomenology and experimentally confirmed for tungsten bronze PBN, that PBN and possibly many other tetragonal bronzes can have very high electro-optic coefficients and piezoelectric properties. Furthermore, it has also been observed that a crossover between θ_1 and θ_3 is found to occur in the $Pb_{1-x}Ba_xNb_2O_6$ solid solution family for compositions in the vicinity $x = 0.37$. As shown in Fig. 8, near this composition a morphotropic phase boundary occurs between a ferroelectric orthorhombic (mm 2) and a tetragonal (4 mm) structure. Thus, tetragonal compositions with large θ_1 values and correspondingly large ε_{11} and d_{15} should exist near the morphotropic phase boundary.

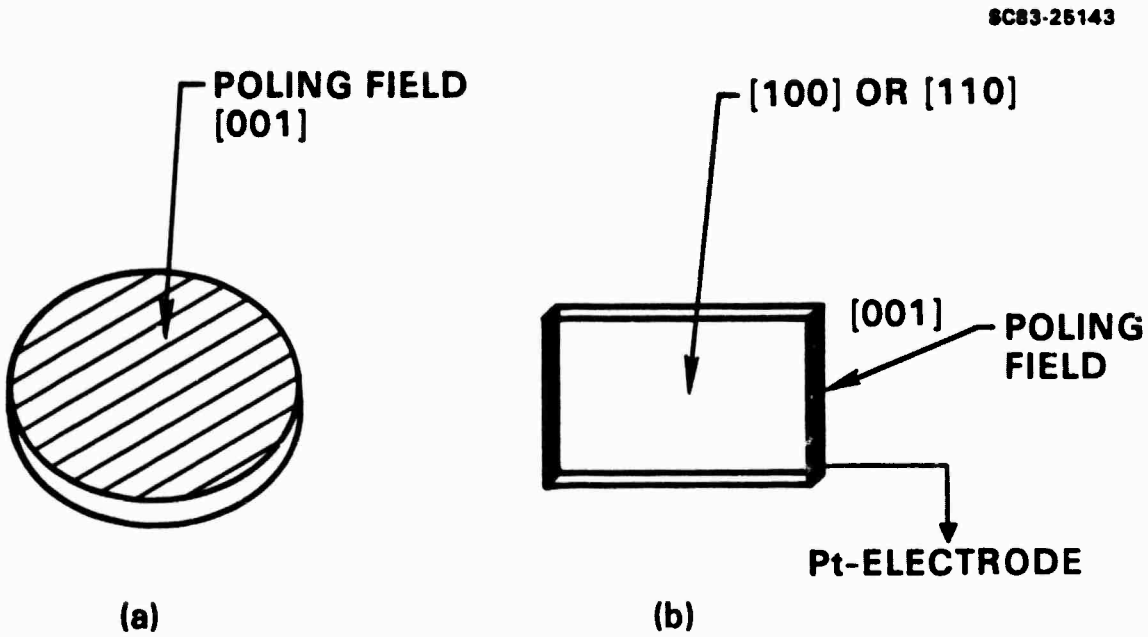

Fig. 7 Poling direction for different orientations.

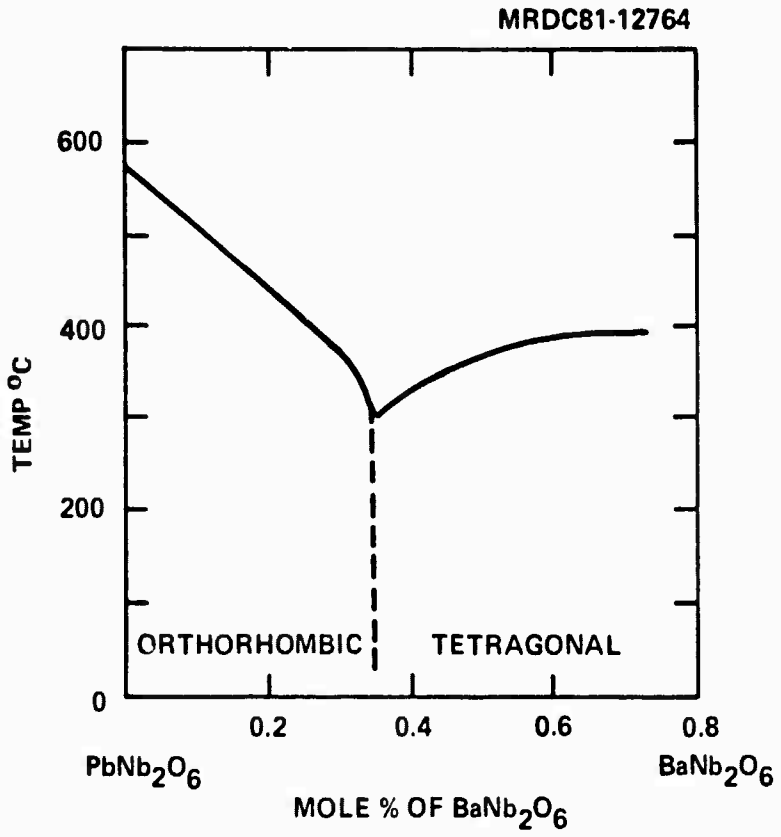

Fig. 8 Phase diagram for the $PbNb_2O_6$-$BaNb_2O_6$ system.

It is the purpose of this investigation to grow thin films in the PBN system near the morphotropic phase boundary, and to identify suitable composition for electro-optics, as well as other device studies. Recent work by Nagata et al[10] and Yokosuka[11] indicated that the electro-optic coefficient increases with the addition of La^{3+} for Pb^{2+}.

Although this system melts congruently and the growth of small crystals by the Czochralski technique under this contract has been shown to be successful at Penn State, growth is difficult due to severe Pb^{2+} losses. The best approach for such materials appears to be the LPE technique so that one can significantly reduce these losses. Since the lattice mismatch between PBN/SBN and PBN/BSKNN crystals is minimal, at least on the a-axis, it is believed that this approach should prove to be beneficial to develop tetragonal ferroelectric PBN compositions for optical studies.

3.5 Solvents for PBN Compositions

Preparation of pure or Ba^{2+}-substituted $PbNb_2O_6$ compositions is complicated by the existence of ferroelectric and nonferroelectric modifications.[12,13] The first is orthorhombic and the latter is rhombohedral, which converts to an orthorhombic ferroelectric form above 1100°C. However, this transition is regarded as reversible and is accompanied by considerable temperature hysteresis. The high temperature ferroelectric form is usually prepared by heating the sample at 1200°C for at least 30 min and then cooling rapidly. In order to use this ferroelectric form for the proposed study, it is important that this transition be lowered so that one can stabilize the ferroelectric form at around 1000°C or lower. At present, efforts are underway to accomplish the following two tasks:

1. Identify a suitable solvent that will lower the ferroelectric/nonferroelectric phase transition temperature.

2. Establish the tetragonal tungsten bronze phase that is compatible with SBN and BSKNN substrates, i.e., maintain a relatively high Ba^{2+} concentration.

There are a large number of solvents that have been identified for PBN. However, the choice in the present work is restricted to only vanadium-containing solvents. The discussion on these solvents and construction of the phase diagram have been given in an earlier report. Three systems based on vanadium, namely $LiVO_3$-PBN, BaV_2O_6-PBN and $Pb_2V_2O_7$-PBN, have been investigated and it was found that the first two systems are unacceptable, since the $LiNbO_3$ and $BaNb_2O_6$ phases remained stable over all temperature ranges.

The third system, $Pb_2V_2O_7$-PBN, appears to be suitable for this work and is now being evaluated. Although the nonferroelectric phase is still being observed, it appears at a slightly lower temperature. When the nonferroelectric rhombohedral phase was heated over 1100°C, the orthorhombic ferroelectric tungsten bronze phase was obtained. However, at this stage, the composition of the PBN phase is not yet identified. Hence, precise lattice constant measurements on these compositions is in progress to identify x in $Pb_{1-x}Ba_xNb_2O_6$. This will allow us to determine the actual concentration of Ba^{2+} in the final composition for film growth.

Since tetragonal tungsten bronze SBN and BSKNN are the only available substrate materials, it is important that the phase crystallized from the $Pb_2V_2O_7$-PBN system also exhibit a tetragonal structure. As shown in Fig. 8, the tetragonal tungsten bronze phase appears below x = 0.40. This indicates that the concentration of Ba^{2+} should be high to maintain the tetragonal phase. Since the BaV_2O_6 solvent shows a tendency to form $BaNb_2O_6$, the present assemblage will be treated on the ternary system as follows:

$Pb_2V_2O_7$-$Ba_2V_2O_7$-PBN.

Although the $Ba_2V_2O_7$ phase does not occur in the BaO-V_2O_5 system, the ternary system will be studied on that formula weight. Work in this direction is in progress, and we expect to produce Ba^{2+}-rich PBN compositions in the near future. The present authors have already successfully shown the growth of $Li_{1-x}Na_xNb_2O_6$ films using the $LiVO_3$-$NaVO_3$-$LiNbO_3$ ternary system.[14,15]

3.6 Summary

We have successfully demonstrated LPE growth of the SBN:40 bronze composition and the poling of SBN:60 substrates. Also developed is a new subsystem, $Pb_2V_2O_7$, for future film growth. Areas of research in the next six months are:

- Establish $Pb_2V_2O_7$:BaV_2O_7:PBN system to yield the tetragonal tungsten bronze phase.
- Establish the poling technique for film/substrate grown on (100) and (110) orientations.
- Develop the surface finish necessary for device studies.

Plans are made to study these problems to decide the applicability of these films for device studies. We believe that film poling will be a critical task in this work and will require full attention. At present, films grown on (001) plates are slightly rougher due to lattice mismatch, and this problem has to be studied in more detail using current substrates or other bronze crystals. Bronze SBN:50 (under DARPA contract) and BSKNN (under NVL and ONR contracts) crystals are being grown, and as soon as suitable size crystals become available, we expect that we will have a good selection of substrate material for LPE work. This will speed up our work and should make it possible to develop different films for electro-optic applications.

4.0 ELECTRO-OPTIC CHARACTERIZATION OF TUNGSTEN BRONZE PBN AND SBN CRYSTALS

4.1 Introduction

In the previous report, phenomenological relations were developed for the linear electro-optic constant, r_{ij}, of the tetragonal ferroelectric tungsten bronze structure crystals. The equations permit a simple description of the symmetry permitted r_{ij}'s in terms of the quadratic electro-optic g_{ij} constants of the prototype paraelectric phase, the spontaneous polarization in the ferroelectric phase, P_3, and the appropriate components of the dielectric tensor, ε_{ij}, i.e.

$$r_{13} = 2g_{13}P_3\varepsilon_{33} \tag{1}$$

$$r_{33} = 2g_{33}P_3\varepsilon_{33} \tag{2}$$

$$r_{42} = r_{51} = g_{44}P_3\varepsilon_{11} \tag{3}$$

The advantage of the derivation is that the prototypic g constants are only very weak functions of temperature so that the relations clearly point up the importance of controlling and enhancing P and ε to achieve large r constants.

Data for ten different bronze compositions were assembled and the $(g_{33}-g_{31})$ and g_{44} constants derived by measurement of the birefringence and spontaneous polarization. From the g constants, values were calculated for $r_{33}-r_{31}$ and for $r_{51} = 4_{42}$. The most important conclusion was that for compositions in the lead barium niobate (PBN) family in the tetragonal ferroelectric region, but close to the morphotropic phase boundary near the 60:40 composition, very high and almost temperature independent values of ε_{11} can contribute very large values of r_{51}.

The tasks taken up in the current contract period were to extend the crystal growth work so as to move in closer to the MPB from the tetragonal side, and to verify by direct measurement the expected very high values of r_{51} and r_{42}. In the former task, work is progressing smoothly, and an additional composition closer to the MPB has been grown and characterized. For the measurements of r_{51}, we are having difficulty in making precise measurements due to an apparent sensitivity to the poling conditions.

While this is being tackled, we have made measurements of the necessary dielectric and pyroelectric properties, and have characterized the comparable piezoelectric d_{15} and d_{24} constants. Data for these measurements, together with preliminary data for the r constants, is presented.

4.2 Experimental Data

4.2.1 Growth of $Pb_{1-x}Ba_xNb_2O_6$ Crystals

The materials used in growth were Specpure PbO, $BaCo_3$ and Nb_2O_5 from Johnson Matthey in England. Chemicals were weighed out to the stoichiometry required, then excess lead added. In each case, the chemistry of the finally grown crystal was determined by chemical analysis, and the composition changes across the phase diagram produced by successive iterations.

The mixed oxides were wet ball-milled in ethanol, then prefired in Al_2O_3 crucibles at 650°C for 24 h before being loaded into the 40 mm diameter Pt pulling crucible. Growth was by Czochralski method in an RF heated Crystallox pulling system. Typical conditions were pulling rates ~ 2 mm/h with rotation at 10 rpm. For initial runs, the objective was not to grow large perfect crystals, but to produce a family of small boules from which uncracked sections could be cut to give representative samples for several different stoichiometries. Typical boules produced were cracked, even on very slow cooling, but contained sections with dimensions up to 10 x 5 x 8 mm, adequate for characterization studies.

Chemical analysis revealed significant departures in the as-grown samples from the initial starting stoichiometry, and in each case, the chemically determined actual crystal stoichiometry is given. Compositions which have been grown to a size suitable for measurement are shown in Table 5.

X-ray powder diffraction analysis was used to determine the symmetry and the lattice parameters. The symmetry change from tetragonal to orthorhombic on crossing the MPB compositions was confirmed by the optical character in polarized light.

4.2.2 Property Measurement

To determine the necessary dielectric, piezoelectric and electro-optic properties, plate bar and cube shaped samples were cut with major surfaces normal to a and c (1 and 3) axes of the tetragonal crystals with $x > 0.4$. For compositions in the orthorhombic ferroelectric phase, samples were cut with major faces perpendicular to the orthorhombic a and b axes, which make an angle of $\simeq 45°$ between the tetragonal a axis.

Sputtered Au electrodes were used, and the crystals were poled by slow cooling under dc fields of 1-2 kV/cm along the c axis for tetragonal species, and along the b axis in orthorhombic crystals. This poling process appears perfectly adequate for the measurement of the piezoelectric d constant, both d_{33} and d_{15}, and since these are related to the Q, P_3 and ε in exactly the same manner as the r constants, we have gone ahead and made the valuation. The problem for r constants appears related to the much larger E fields we have been using, and to the fact that our initial sample cuts are slightly misoriented ($\sim 5°$) away from the c axis.

New samples are now being cut and poled for the r measurements. The characterization of dielectric, pyroelectric and piezoelectric parameters for the samples are given in Table 5.

Table 5

Physical Properties of Ferroelectric $Pb_{1-x}Ba_xNb_2O_6$

Composition	Density (g/cc)	Lattice Parameters (Å) a	b	c	Curie Temp. and Const. T_c°C	C_1 (x 10^{-5}°C) -1		Dielectric Constant K_a	K_b	K_c	Piezo Coefficient (x10^{12} C/N) d_{33}	d_{15}	Pyroelectric (x10^4 C/m²°C) p
$Pb_{.33}Ba_{.70}Nb_{1.99}O_6$	5.65 (5.92)(a)	12.500		3.995	350	-120	1.9	360 (400)(b)		140 (40,000)(b)	60	52	1.7
$Pb_{.37}Ba_{.53}Nb_{2.04}O_6$	5.72 (5.82)	12.486		3.980	430	150	2.0	630 (800)		80 (37,000)	65	112	0.9 (1.4) (c)
$Pb_{.60}Ba_{.42}Nb_{1.99}O_6$	6.05 (6.17)	12.495		3.989	352	240	2.1	1600 (2000)		200 (20,000)	110	250	0.9
$Pb_{.56}Ba_{.40}Nb_{2.02}O_6$	6.10 (6.12)	12.480		3.970	367	250	2.3	1600 (2600)		210 (18,000)	140	310	0.7 (0.9)
$Pb_{.56}Ba_{.44}Nb_{2.00}O_6$	6.10 (6.13)	12.499		3.971	315	300	2.4	2500 (2800)		350 (35,000)	185	380	1.3 (0.6)
$Pb_{.86}Ba_{.19}Nb_{1.98}O_6$	6.45 (6.52)	17.67	17.92	7.78	430	---	3.6	1200 (16,000)	225 (16,000)	1900 (2,000)	70	<500	2.1
$PbNb_2O_6$	(6.6)	17.65	17.92	7.74	560	---	4.0	500 (23,000)	400 (23,000)	1000 (1,200)			

(a) Calculated density (b) Peak value at T_c (c) Pyroelectric value assuming T_c = 350°C

4.2.3 Preliminary Linear Electro-Optic Measurements

For a field E_1 applied orthogonal to the c axis, the change in the principal birefringence is given by

$$\Delta n_i = -\frac{1}{2} n^3 r_{51} E_1 \quad . \tag{4}$$

Using the conoscopic figure for a SBN:60 crystal for a field $E_1 = 5 \times 10^5$ V/meter, the measured change of birefringence $\Delta n_i \simeq 2 \times 10^{-4}$, giving a value of r_{51}

$$r_{51} = 0.8 \times 10^{-10} \text{ m/V} = 80 \times 10^{-12} \text{ m/V}$$

Table 6 summarizes the dielectric, piezoelectric and electro-optic properties of the tungsten bronze system $Sr_{1-x}Ba_xNb_2O_6$, $.25 < x < .75$. It is known that r_{33} is highest (1350×10^{-12} m/V) for the $Sr_{.75}Ba_{.25}Nb_2O_6$ (SBN:75) composition, and decreases as the Ba content is increased. Although r_{13} also decreases, the behavior of $r_{51} = r_{42}$ is considerably different. The present measurements show that r_{51} actually increases with increasing Ba^{2+} content, being substantially larger for SBN:60 (80×10^{-12}) as compared to SBN:75 (42×10^{-12}). This result indicates a strong compositional dependence for

Table 6

Electro-Optic Behavior in the Tungsten Bronze $Sr_{1-x}Ba_xNb_2O_6$ System

Property	SBN:75	SBN:60	SBN:50
Curie Temp (°C)	56	72	125
Dielectric Constant	$\varepsilon_{33} = 3400$	$\varepsilon_{33} = 600$	$\varepsilon_{33} = 500$
Electro-Optic Coef. m/V	$r_{33} = 1350$ $r_{13} =$	$r_{33} = 420$ $r_{13} =$	$r_{33} = 180$ $r_{13} =$

r_{51}, but in a manner opposite to that of r_{33}. Since SBN:50 single crystals are now available from this work, it would be interesting to investigate the magnitude of r_{51} in this composition to see if it is greater than that measured for SBN:60. This should contribute important information regarding the potential of SBN for optical switching applications and spatial light modulators.

4.3 Discussion

For the piezoelectric constants, the phenomenological equations are

$$d_{15} = Q_{44} P_s \varepsilon_o K_a \tag{5}$$

where Q_{44} is the quadratic shear electrostriction constant in the paraelectric prototype. This may be compared to the electro-optic equation

$$r_{51} = g_{44} P_s \varepsilon_o K_a \quad . \tag{6}$$

Since both Q_{44} and g_{44} are only weak functions of temperature, d_{15} and r_{51} should have similar temperature characteristics, depending on the same manner upon P_s and ε_{33}.

From Table 5, the benefit of the MPB is very apparent in the very large values of ε_{11} which occur at temperatures well below T_c, where P_3 is also very large. For a further test of the phenomenology, one may derive an expression for the dielectric stiffness, χ_{11}, from the Devonshire theory in the form

$$\chi_{11} = \frac{1}{\varepsilon_{11}} = \frac{T-\theta_1}{C\varepsilon_o} + 2\alpha_{13} P_3^2 + 2\alpha_{133} P_3^4 + 2\alpha_{1333} P_3^6 \quad . \tag{7}$$

Using values of $C = 2.0 \times 10^5$°C and value for the α constants derived in earlier studies of SBN[16], ε_{11} at room temperature can be calculated as a function

of the transverse Curie temperature, θ_1. In Fig. 9, calculated and measured values of K_a (ε_{11}) are compared for compositions with different θ_1 values. In the same graph, values of d_{15} are also added, indicating the dominant role of K_a for temperatures remote from T_c.

.4 Conclusion

The piezoelectric and dielectric measurements on compositions in the lead barium niobate bronze ferroelectrics agree closely with the expectations of phenomenological theory. Preliminary data for the r_{51} also fit well, but more precise data are required to complement and confirm the theory. These measurements will be completed in the next quarter.

The theoretical curve underscores the importance of obtaining crystals with tetragonal compositions very close to the MPB, and additional effort is being focused upon this aspect of the work.

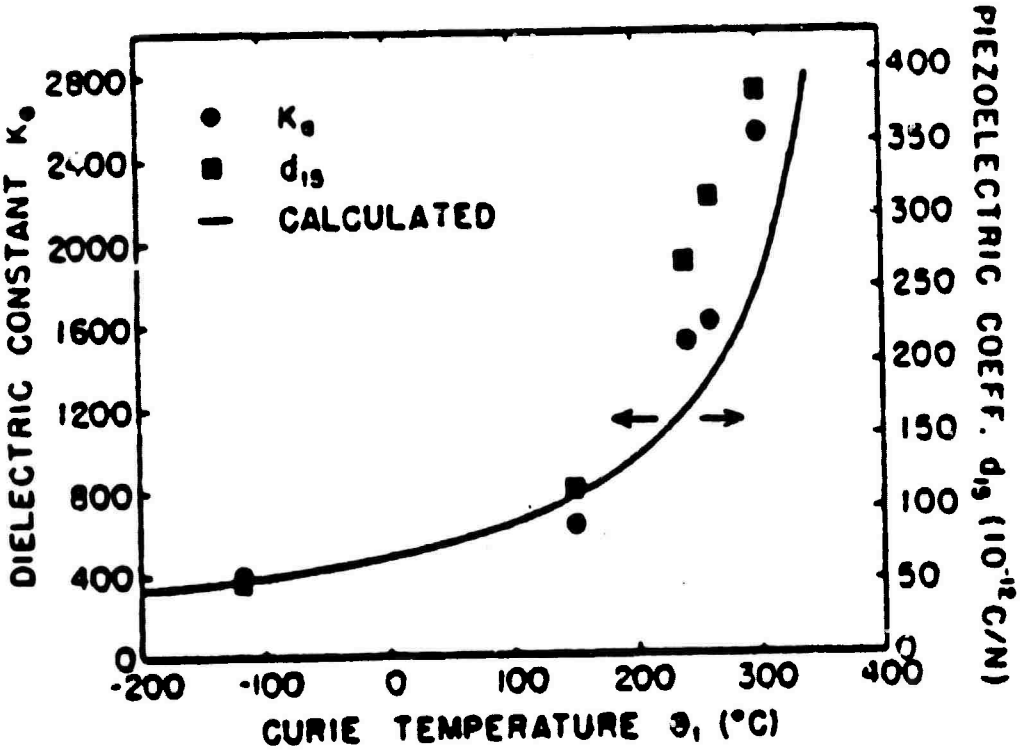

Fig. 9 Measured and calculated room temperature dielectric and measured piezoelectric parameters as a function of transverse Curie temperature θ_1 in PBN compositions.

5.0 NEW TUNGSTEN BRONZE SYSTEMS FOR ELECTRO-OPTIC STUDIES

Several of the most interesting tungsten bronze systems show morphotropic phase boundaries (MPB) which depend primarily on composition rather than on temperature. Ceramic or single crystal compositions adjacent to such boundaries show considerable enhancement of electro-optic, dielectric, piezoelectric, electromechanical and pyroelectric properties because of the proximity in energy of an alternate ferroelectric structure. In the present work, two such systems, $BaNaNb_5O_{15}$-$Sr_2NaNb_5O_{15}$ and $Pb_2KNb_5O_{15}$-$BaNaNb_5O_{15}$, have been developed and are found to have MPB conditions with exceptionally high dielectric and other properties. The present report includes information on these systems as a starting point for future materials for electro-optics and other device applications.

5.1 $Ba_2NaNb_5O_{15}$-$Sr_2NaNb_5O_{15}$ System

Tungsten bronze barium sodium niobate (BNN) has been shown to be an outstanding material for electro-optic and nonlinear optic applications, particularly for second harmonic generation of near-IR laser radiation. The material was first discovered in 1967 by researchers at Bell Labs,[17] and was found to have a number of useful nonlinear optic and piezoelectric properties. Stoichiometric $Ba_2NaNb_5O_{15}$ is orthorhombic at room temperature with lattice constants a = 17.592Å, b = 17.626Å and c = 3.995Å, as determined from high angle x-ray measurements.[18] Because of the small difference between a and b, routine x-ray powder diffraction measurements show a tetragonal structure. Above 260°C, an orthorhombic to tetragonal transformation occurs in which microtwinning is usually observed in single crystals, but with no significant dielectric anomalies. The Curie point is at approximately 570°C.

Based on our earlier theoretical work on the tungsten bronze family[19] and experimental work on $Pb_{1-x}Ba_xNb_2O_6$, an enhancement of the piezoelectric, pyroelectric and electro-optic properties can be anticipated for tungsten bronze compositions which exhibit a morphotropic boundary condition between

tetragonal and orthorhombic phases. Furthermore, a reduction in the Curie temperature is also highly desirable. To this end, we have begun an investigation of the pseudo-binary system $(1-x)Ba_2NaNb_5O_{15}$-$(x)Sr_2NaNb_5O_{15}$ in which some of the Ba ions are replaced with Sr via the inclusion of $Sr_2NaNb_5O_{15}$ (SNN).

Materials were prepared by the normal procedure of mixing, calcining at 900-950°C, then ball-milling for 12-18 h. The cold pressed slugs were then sintered for 2 h at 1250-1280°C, depending on the composition. The ceramic disks were then polished and platinum electrodes were vacuum deposited for dielectric characterization. The results for the variation in the Curie point, T_c, as a function of composition are shown in Fig. 10. A significant drop in T_c is seen for even small amounts of SNN ($x > 0.1$). Optical evaluations by Van Uitert et al[20] on single crystals in this compositional system have shown a pseudo-tetragonal structure at room temperature over the range $0 < x \leq 0.75$, with a broad Curie point minimum at 210°C for $x \simeq 0.75$. Powder x-ray diffraction measurements in this work show a tetragonal structure up to $x \simeq 0.6$ at which point a sharp minimum in T_c (170°C) occurs. The differences observed can be primarily attributed to the large deviations from stoichiometry for the Czochralski grown crystal used in the work by Van Uitert et al.[20] The use of ceramic samples in the present work, with lower sintering temperatures for growth and low weight loss (typically 1-2%), insures compositions which are much closer to true stoichiometry. Beyond the $x = 0.6$ point, the compositions show a gradual rise in T_c to 260°C for pure SNN. Dielectric data for compositions close to SNN do not show the broad, low dielectric peak at 150-200°C previously reported,[20] but do indicate the onset of a second peak well below room temperature for compositions with $x > 0.65$.

Dielectric data for the BNN-SNN system are shown in Fig. 11. A sharp rise in the dielectric constant, K, at room temperature and at T_c is seen for compositions in the range of $0.6 \leq x \leq 0.7$. The gradual rise in the room temperature dielectric constant near the pure SNN composition is a result of the previously mentioned low temperature peak; for SNN ($x = 1$), the dielectric

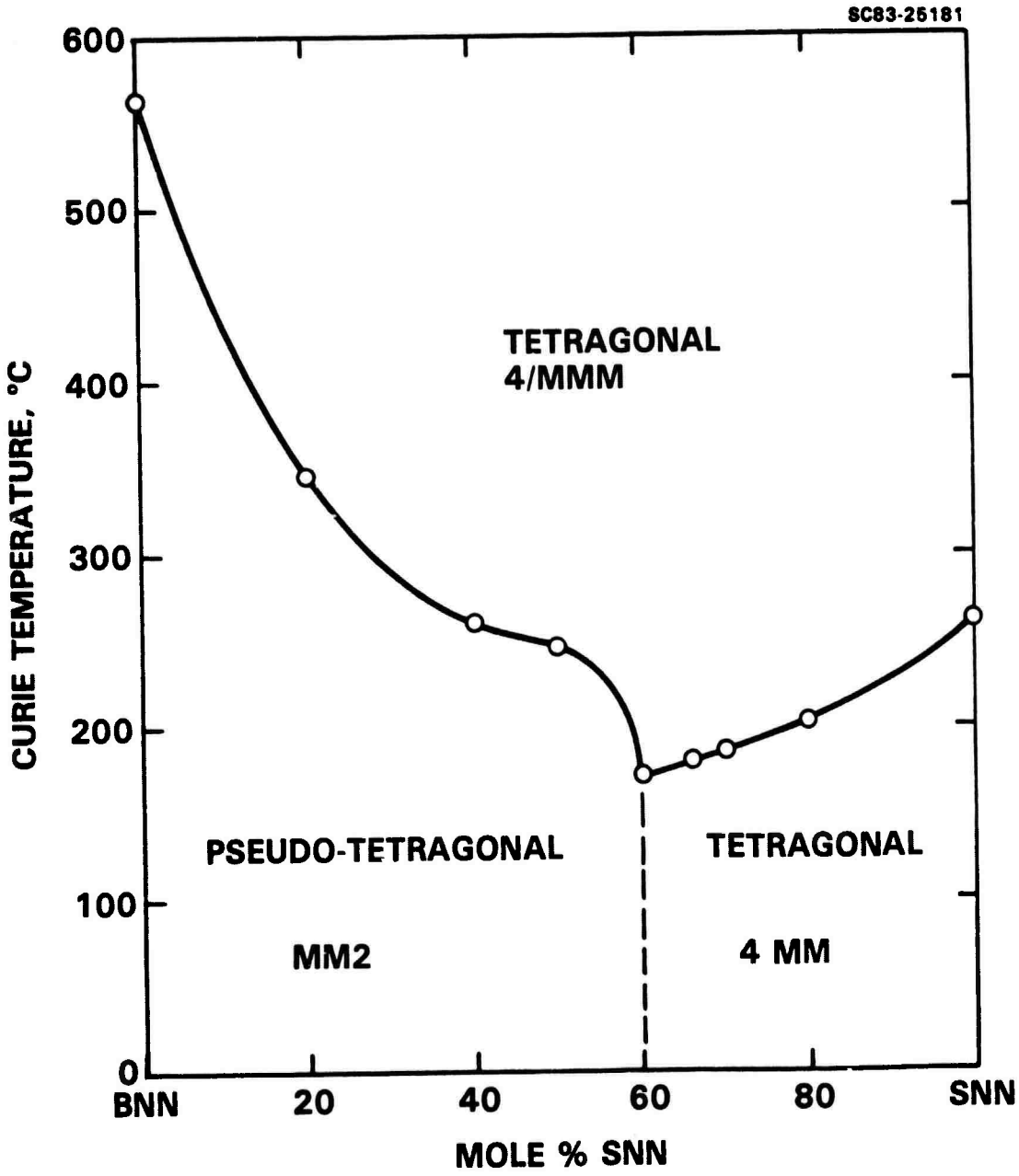

Fig. 10 Morphotropic phase boundary conditions for the system BNN-SNN.

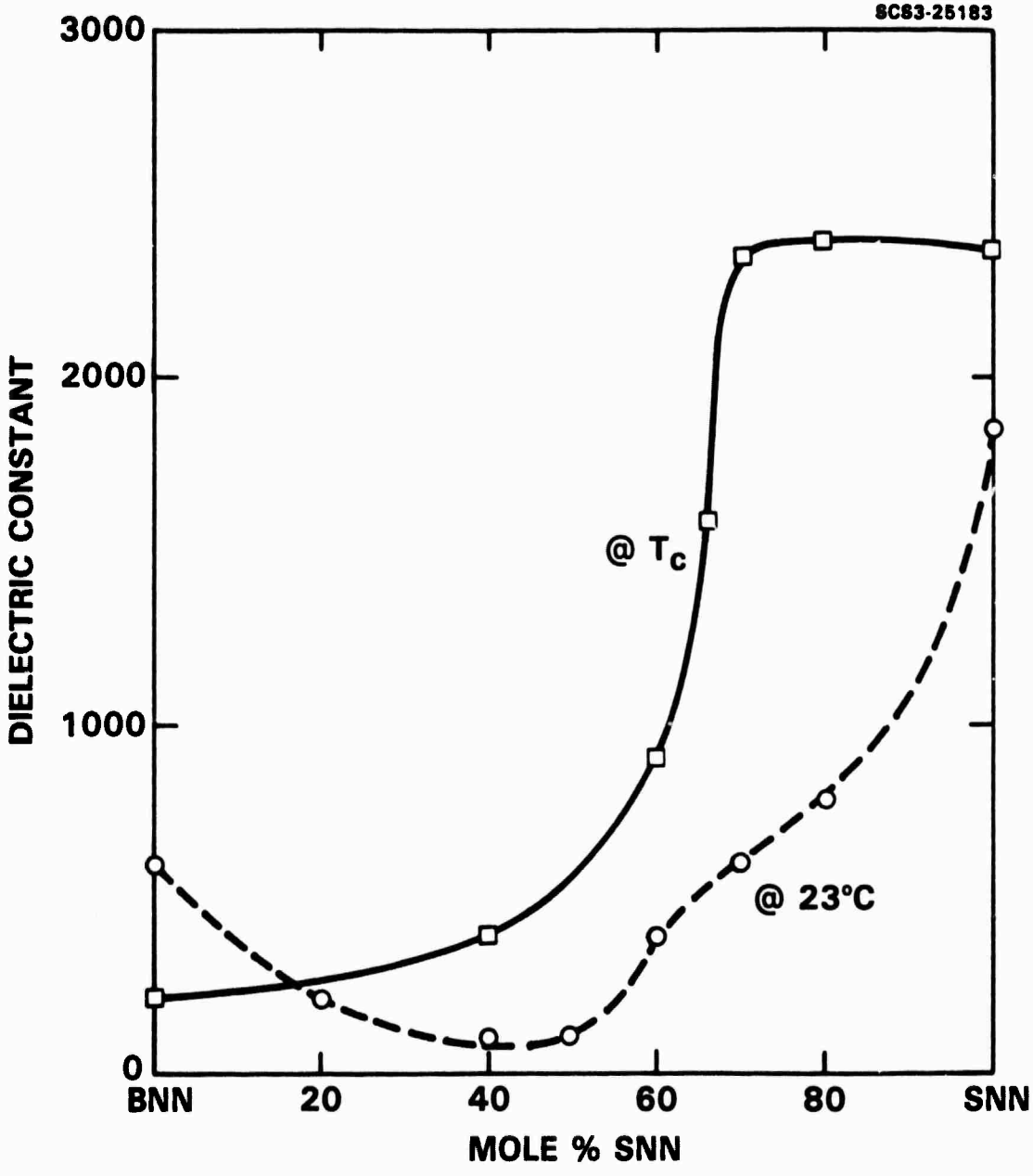

Fig. 11 Variation of room temperature and Curie point dielectric constant as a function of composition for the system BNN-SNN.

constant was observed to decrease from its room temperature value as the sample was warmed until the onset of the ferroelectic transition peak.

These data are considered preliminary at this time due to the sensitivity of this system to sintering temperature, particularly for the range $0.4 < x < 0.8$. Work is continuing on the refinement of the dielectric and structural characterization of this system. Of particular interest is the nature of the structural change near $x = 0.6$, since both BNN and SNN show pseudo-tetragonal structures.

5.2 $Pb_2KNb_5O_{15}$-$Ba_2NaNb_5O_{15}$ System

Another tungsten bronze of interest is $Pb_2KNb_5O_{15}$ (PKN). This composition has been successfully grown in hot-pressed dense ceramic form by Nagata et al[21] in Japan with a high electrochemical coupling constant, k_t = 0.40, and good polarization. As such, it represents an attractive candidate for SAW, piezoelectric and pyroelectric device applications. However, its relatively high Curie point (470°C) makes it very difficult to completely pole. It is also prone to cracking above 1200°C growth temperatures,[21] and hence the attainment of optically transparent hot-pressed material remains unlikely.

Ceramic PKN prepared in this laboratory shows an orthorhombic structure with a = 17.835Å, b = 17.944Å and c = 3.938Å, these values being determined from powder x-ray analysis with an excellent fit to 28 lines. The orthorhombic structure of PKN presents the possibility of attaining a morphotropic phase boundary condition in combination with another tetragonal or pseudo-tetragonal tungsten bronze composition such as BNN. To this end, we have initiated study of the pseudo-binary system, $(1-x)Pb_2KNb_5O_{15}$-$(x)Ba_2NaNb_5O_{15}$, using cold-pressed and sintered ceramic samples. The 10 KHz dielectric data for the Curie point, T_c, as a function of composition for the system PKN-BNN are shown in Fig. 12. A sharp drop in T_c is observed for the composition, (.75)PKN-(.25)BNN, at which T_c = 265°C. For higher percentages of BNN, the Curie point rises smoothly to the upper value of 565°C at the end

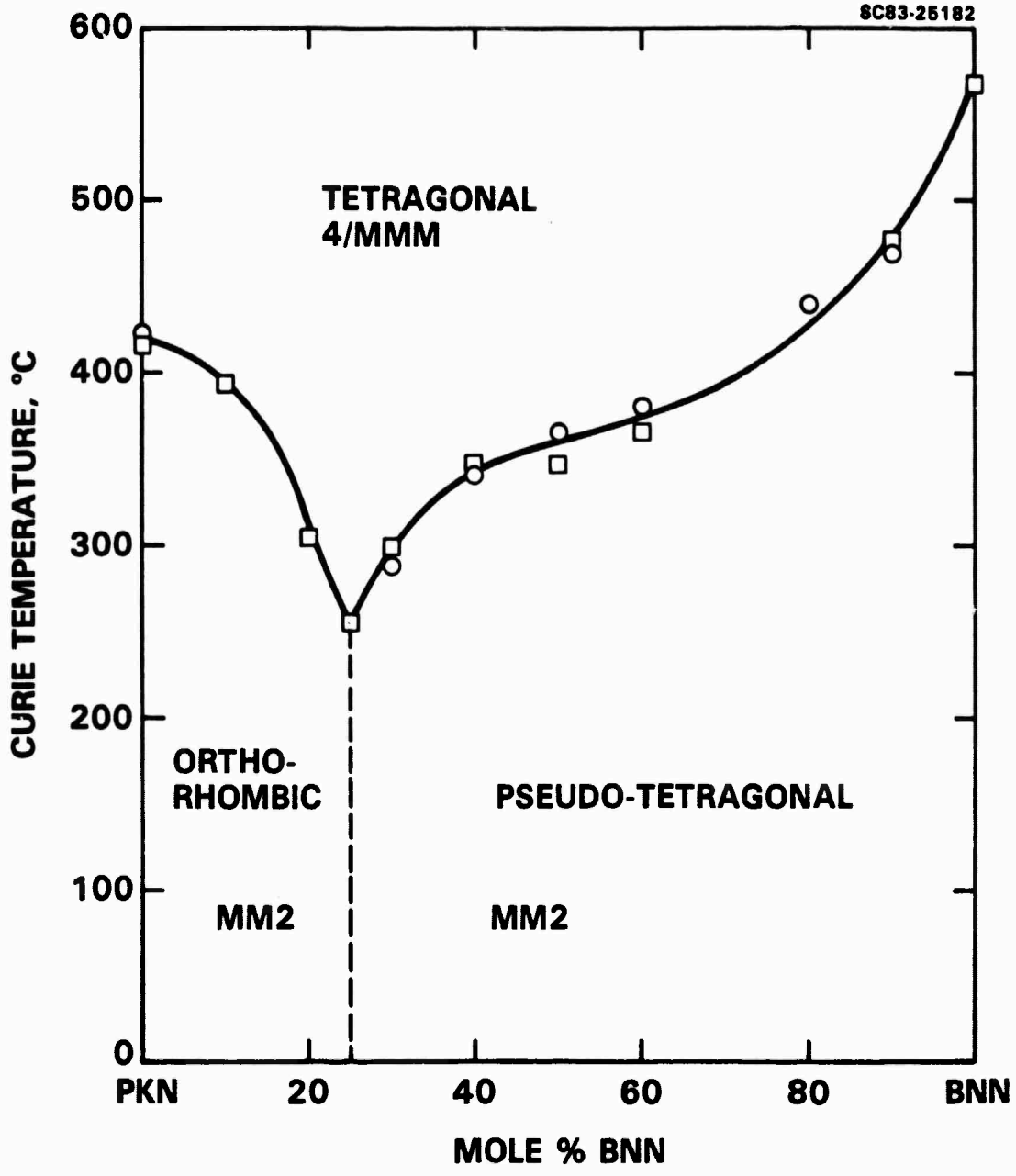

Fig. 12 Morphotropic phase boundary conditions for the system PKN-BNN.

point. Data for the dielectric constant at room temperature and at T_c as a function of composition (Fig. 13) show a sharp maximum in the r-t dielectric value at x = 0.25, with a corresponding steep drop in the value at T_c. The dielectric constant at T_c for pure PKN (11,700 at 420°C) corresponds very well with the average fo the peak dielectric constants measured in hot-pressed PKN for cuts made perpendicular and parallel to the pressing direction (13,800) reported by Nagata et al.[21] Hence, aside from grain orientation effects in hot-pressed material, further densification does not appear to significantly improve the dielectric properties of PKN.

Microcracks in the normally sintered ceramics were a significant problem over much of the compositional range. Compositions with a large percentage of PKN showed substantial cracking when sintered at 1200°C for 2 h, with the samples often crumbling during subsequent measurement. This problem was alleviated by sintering at 1180°C for 4 h, although widely dispersed microcracks could still be observed in some samples. Curiously, no microcracks were observed for samples in the morphotropic boundary region, $0.2 < x < 0.3$. For larger values of BNN content, it was necessary to progressively raise the sintering temperature in order to obtain good ceramic densities. The dielectric properties, particularly at Curie point, appeared very sensitive to sintering conditions for compositions near the morphotropic boundary; hence, these data still need some refinement.

Further work is planned for this compositional system in the coming months, including continued x-ray structural analysis, dielectric measurements, and piezoelectric characterization of poled samples with morphotropic and near-morphotropic compositions. The present data indicate potential use of this system in piezoelectric, millimeter wave and SAW device applications. Tetragonal near-morphotropic compositions of PKN-BNN may also find use in hot-pressed form for electro-optic applications if the apparent greater mechanical stability of these compositions can be used to an advantage to obtain optically transparent material at higher growth temperatures. The pseudo-binary system, $(1-x)Pb_2KNb_5O_{15}$-$(x)Sr_2NaNb_5O_{15}$, will also be investigated as an

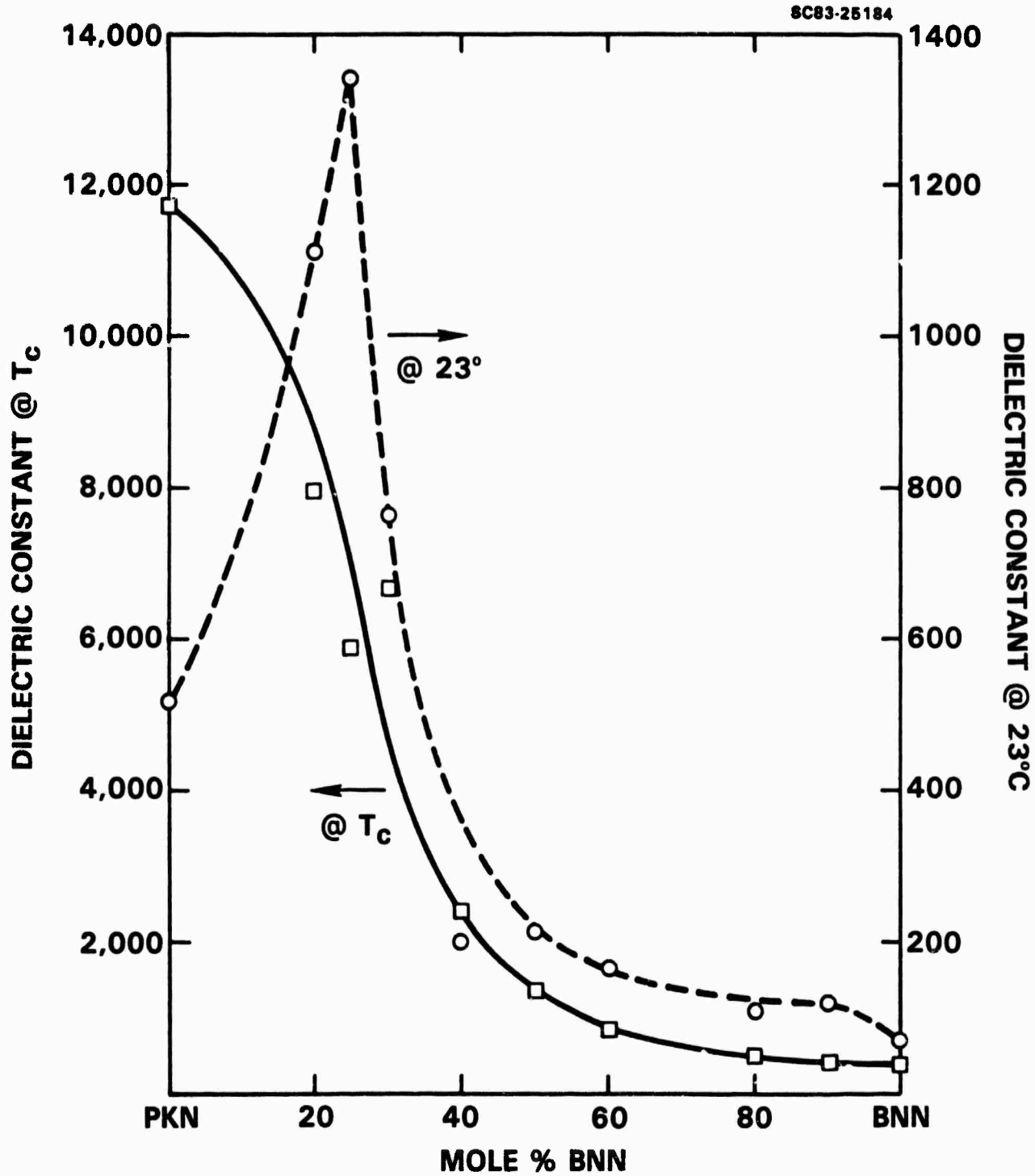

Fig. 13 Variation of room temperature and Curie point dielectric constant as a function of composition for the system PKN-BNN.

alternative to the present system, since the replacement of the improper ferroelectric BNN by ferroelectric SNN may result in a number of interesting changes and/or enhancements in the ferroelectric properties, particularly near morphotropy.

Both the PKN-BNN and BNN-SNN systems have been shown to be promising for electro-optic, pyroelectric and millimeter wave device application studies. A few compositions exhibit enhanced dielectric properties at room temperature and at T_c. Some of these will be selected for single crystal Czochralski growth and the ferroelectric and electro-optic properties will be established in greater detail. Based on this work, necessary modification in the system compostion will be made in order to achieve optimum optical properties for waveguide, electro-optic modulator and ohotorefractive applications.

6.0 PHOTOREFRACTIVE TUNGSTEN BRONZE CRYSTALS FOR NONLINEAR OPTICS

The development of photorefractive tungsten bronze single crystals is a recent addition to the current project, and this task has been initiated as of October 1, 1983. This report includes our overall task objectives and also presents some current results on SBN:60 crystals.

6.1 Objective

Selective doping of $Sr_{1-x}Ba_xNb_2O_6$, x = 0.40 an 0.25, crystals has been shown to produce significant photorefractive effects, and this solid solution offers many possiblities for further improvements. The objective of this program is to develop and study optical quality, doped $Sr_{1-x}Ba_xNb_2O_6$ (SBN) or other tungsten bronze crystals. The photorefractive sensitivity and speed of doped SBN single crystals will be investigated with respect to current need for their possible application in real time image processing and for holographic storage media. In addition, a suitable phenomenological model will be developed to explain the influence of the ferroelectric characteristics and the role of impurity ions in controlling the photorefractive sensitivity and response (speed) in ferroelectric tungsten bronze and other structural families.

6.2 Importance of Tungsten Bronze Family Crystals

There are several interesting ferroelectric structural families (perovskite, ilmenite, BSO, etc.) that exhibit excellent electro-optic properties, but the tungsten bronze family crystals, such as $Sr_{1-x}Ba_xNb_2O_6$ (SBN:75 and SBN:60), $Ba_{2-x}Sr_xK_{1-y}Na_yNb_5O_{15}$ (BSKNN), $Sr_2KNb_5O_{15}$, and $Pb_{1-x}Ba_xNb_2O_6$ (PBN), appear to be more attractive candidates for the proposed work because of the following features:

1. Tungsten bronze family crystals possess very high electro-optic coefficients.

2. Large size (over 1 in. diameter) and optically good quality crystals are available, e.g., SBN, BSKNN, etc.

3. The open structure of the tungsten bronzes will accommodate a wide range of single or multiple dopant species.

4. Compositional flexibility permits modification of refractive index and other key properties of the host.

Table 7 summarizes the electro-optic and ferroelectric properties of selected tungsten bronze compositions. Since materials development is the major part of the proposed research and development program, much of the effort will be expended in the growth and characterization of selected crystals with and without dopants. Initially, emphasis will be placed on two areas:

1. Growth of defect-free undoped SBN:60 and other tungsten bronze single crystals of suitable size.

2. Determination of the role of suitable dopants on the photorefractive properties of SBN and other bronzes with respect to their valence state and distribution over the different crystallographic sites. This work will initially be done with presently available single crystals in parallel with the development of defect-free growth of bronze crystals.

Table 7

Electro-Optic and Ferroelectric Properties of Tungsten-Bronze Crystals

Composition	Electro-Optic Coefficient (m/V)	Dielectric Constant	T_c (°C)	Crystal Size (Diameter)
$Sr_{0.75}Ba_{0.25}Nb_2O_6$	$r_{33} = 1350 \times 10^{-12}$	3400	56	1-1.5 cm
$Sr_{0.6}Ba_{0.4}Nb_2O_6$	$r_{33} = 420 \times 10^{-2}$	880	72	3 cm
$Sr_{0.5}Ba_{0.5}Nb_2O_6$	$r_{33} = 180 \times 10^{-12}$	440	120	2.5 cm
$Ba_{2-x}Sr_xK_{1-y}Nb_5O_{15}$	$r_{33} = 540 \times 10^{-12}$	600	203	1-1.5 cm
$Sr_2KNb_5O_{15}$	$r_{33} = 280 \times 10^{-12}$	500	150	0.5-0.8 cm
$K_3Li_2Nb_5O_{15}$	$r_{33} = 78 \times 10^{-12}$	100	405	0.5-1.0 cm
$Ba_6Ti_2Nb_8O_{30}$	$r_{33} = 440 \times 10^{-12}$	200	250	0.5-0.7 cm
$Pb_{1-x}Ba_xNb_2O_6:La^{3+}$	$r_{33}^* = 460 \times 10^{-12}$	650	350	Disk & Crystal

* r_{33} obtained on hot-pressed dense ceramic.

6.3 Current Status of SBN:60 Crystals for Photorefractive Studies

The present single crystal growth work has focused on SBN:60. The recent development of striation-free SBN:60 crystals will have a significant impact on this work, and hence, more detailed reserach on this crystal has been planned. Recently, four SBN:60 samples (shown in Fig. 14) were characterized with respect to their optical and photorefractive properties. A significant improvement in the optical quality has been accomplished with the growth of these crystals (Fig. 15), specifically with regard to the minimization of diffraction from striations and overall scattering from defects, etc. The results summarized in Fig. 15 were obtained by propagating a small diameter (~ 1 mm), low intensity (~ 0.8 uw) beam of light from an argon ion laser (5145A) along the a-axis of each SBN crystal, polarized parallel to the c-axis. In sample #0, both diffraction and scattering are evident (due to striations), whereas sample #1 shows only scattering and sample #2 is dominated by diffraction. Sample #4 is essentially striation-free and exhibits only a residual amount of scattering.

SC84-25779

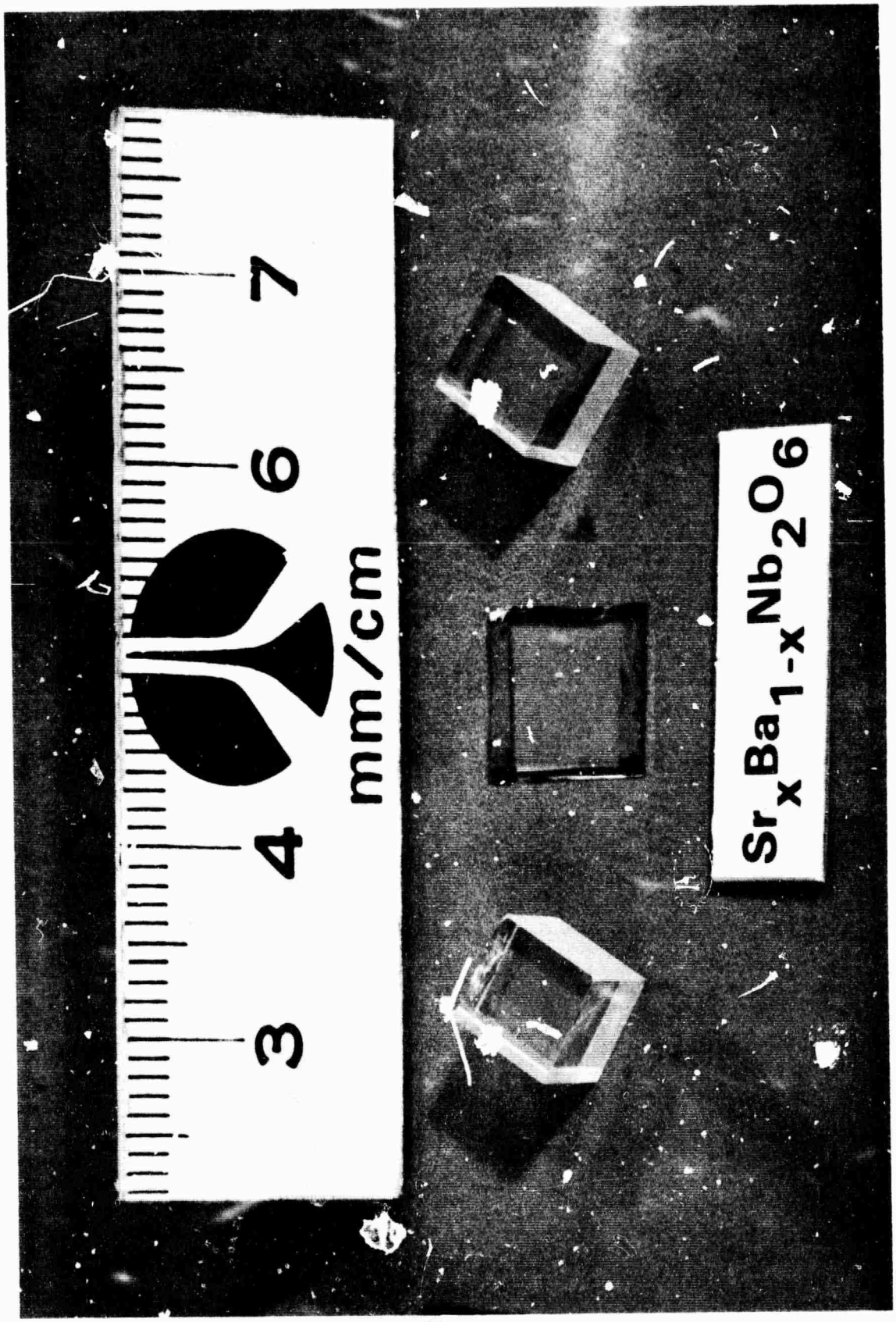

Fig. 14 Different size and shape SBN:60 crystals used for photorefractive studies.

SC83-24554

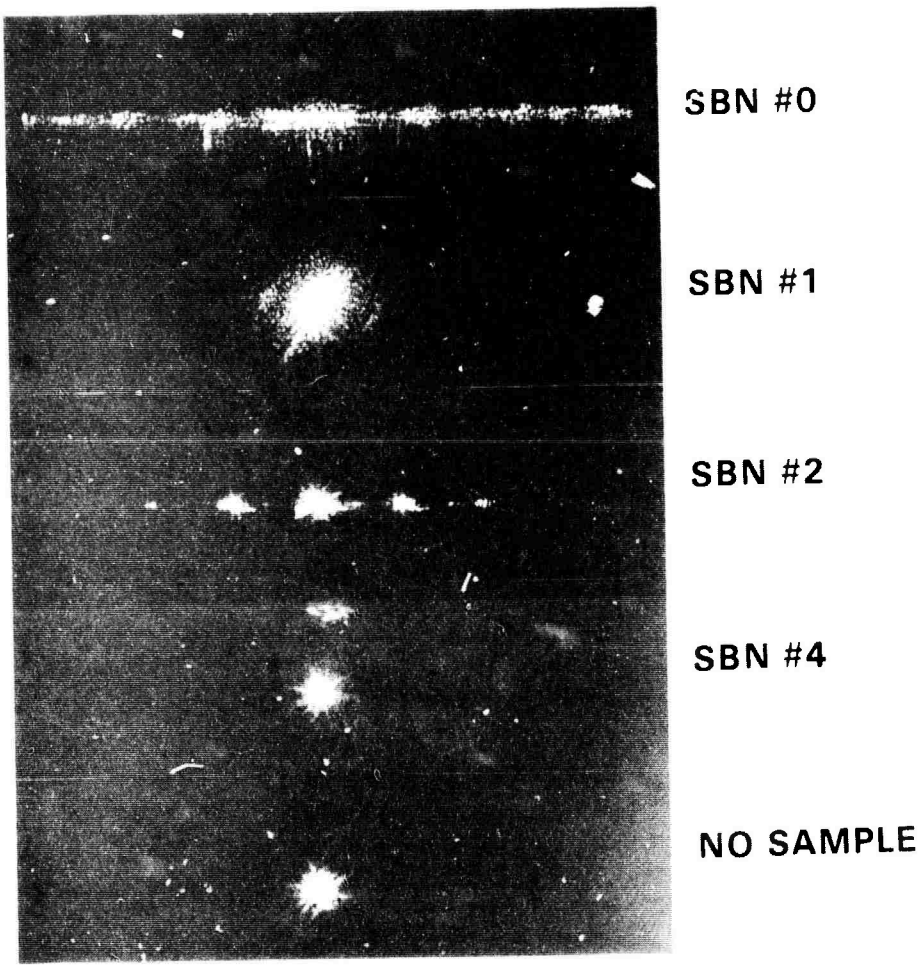

Fig. 15 Diffraction pattern for different SBN:60 single crystals.

Any scattering or diffraction of the type seen in samples #0 1 and 2 of Fig. 15 can seriously impact quantitative optical measurements in these crystals. However, the improved optical quality of SBN:60 observed in sample #4 was sufficient to permit various optical experiments to be performed. These measurements included nonlinear optical two- and four-wave mixing along with transmission spectra, and yielded quantitative results for phase conjugate reflection efficiencies, two beam coupling constants, absorption coefficients, and intrinsic bandgap and photorefractive response times for these samples. Further evaluation of these data is in progress, and the results of this investigation will be given in the next report.

6.4 Future Work: Role of Dopants

Since the optical quality and performance of SBN:60 crystals has now been improved, it is important that other factors such as speed and sensitivity be enhanced for this family of crystals. Besides the further development of striation-free crystals, we will also introduce specific impurities into these crystals. The change in the refractive index for a ferroelectric crystal is given by:

$$\Delta n = 1/3\ n^3 r_{ij} E_{ij} \qquad (8)$$

where r_{ij} = electro-optic coefficient and E_{ij} = space charge field. This indicates that both the electro-optic coefficient and space charge field should be increased to develop efficient material for photorefractive device applications. However, for a given crystal, e.g., SBN:60, the electro-optic coefficient is constant. Hence, it is important that the space charge field should be improved using proper dopants.

Recently, Russian[22] and Japanese[23] researchers successfully demonstrated that the photorefractive sensitivity and response time of tungsten bronze SBN:60 ($Sr_{0.6}Ba_{0.4}Nb_2O_6$) crystals can be effectively improved by introducing proper dopants. According to their work,[23] Ce-doped SBN:60 crystals

exhibit an exceptionally high photorefractive sensitivity of 9.5×10^{-3} cm^2/J, a value that exceeds that of Fe-doped $LiNbO_3$ (4×10^{-5} cm^2/J) by more than two orders of magnitude. The response time for these crystals is marginal, but it is substantially faster than for Fe-doped $LiNbO_3$. This work is significant and provides useful direction for future investigations in order to establish the factors controlling both sensitivity and speed.

A summary of the proposed impurity ions and their possible valence states and site preference is given in Table 8. A thorough understanding of dopant valence states, site preference and concentration as it effects material quality, sensitivity and speed is fundamental to the enhancement of the photorefractive properties of bronze compositions such as SBN:60, and will be explored in depth in this work. The growth of Fe^{3+} doped SBN:60 crystals is in progress, and although the results indicate that growth is more difficult than for undoped crystals, small and reasonable quality crystals have already been grown. The crystals are dark yellow in color and exhibit crystal facets similar to those for undoped SBN:60. The effects of Fe^{3+} addition on the ferroelectric phase transition, dielectric constant and other properties are now being evaluated. Once this is accomplished, the crystals will be tested for their nonlinear optical properties.

Table 8

Proposed Dopants for Photorefractive Studies
in SBN and Other Bronze Crystals

Dopants	Valence State	Site Preference for the Proposed Dopants			
		15-Fold	12-Fold	9-Fold	6-Fold
Cerium	Ce^{3+}, Ce^{4+}	Ce^{3+}	Ce^{3+}	Ce^{4+}	Ce^{4+}
Terbium	Tb^{3+}, Tb^{4+}	--	Tb^{3+}	Tb^{4+}	Tb^{4+}
Iron	Fe^{3+}, Fe^{2+}	--	--	Fe^{2+}	Fe^{2+}, Fe^{3+}
Manganese	Mn^{2+}, Mn^{3+}, Mn^{4+}	--	--	Mn^{2+}	Mn^{2+}, Mn^{3+}
Titanium	Mi^{4+}, Ti^{3+}	--	--	--	Ti^{4+}, Ti^{3+}
Molybdenum	Mo^{6+}, Mo^{4+}	--	--	--	Mo^{6+}, Mo^{4+}
Niobium	Nb^{5+}, Nb^{4+}	--	--	--	Nb^{5+}, Nb^{4+}

7.0 FUTURE PLANNED WORK

- Further improve temperature stability using the ADC system in the Czochralski growth unit to grow striation-free SBN:60 crystals.

- Improve and continue the growth of SBN:50 and SBN:75 crystals for use as substrate material.

- Establish the poling technique for epi-films and evaluate the ferroelectric properties, including dielectric, electromechanical, Curie temperature, piezoelectric and elastic.

- Identify suitable tetragonal tungsten bronze compositions in the $Pb_2V_2O_7$-PBN and $Pb_2V_2O_7$-$Ba_2V_2O_7$-PBN systems which are compatible with SBN and BSKNN substrates.

- Further establish ferroelectric data on the BNN-SNN and PKN-BNN systems to identify optimum compositions for bulk crystal growth work.

- Establish the photorefractive properties of SBN:60 crystals, and also identify suitable dopants to enhance the photorefractive sensitivity and speed.

8.0 PUBLICATIONS AND PRESENTATIONS

8.1 Publications

1. T.R. Shrout, L.E. Cross and D.A. Hukin, "Ferroelectric Properties of Tungsten Bronze Lead Barium Niobate (PBN) Single Crystals," to be published in Ferroelectrics.

2. R.R. Neurgaonkar, W.K. Cory and J.R. Oliver, "Growth and Applications of Tungsten Bronze Family Crystals," to be published in Ferroelectrics.

8.2 Presentations

1. R.R. Neurgaonkar, W.K. Cory and J.R. Oliver, "Growth and Applications of Tungsten Bronze Family Crystals," presented at the 1983 IEEE Int'l. Symp. on Applications of Ferroelectrics, June 1-3, 1983, Gaithersburg, MD.

2. R.R. Neurgaonkar, J.R. Oliver and L.E. Cross, "Growth and Application of Ferroelectric Tungsten Bronze Family Crystals," presented at the 5th European Mtg. on Ferroelectrics, Sept. 26-30, 1983, Benalmadena, Spain.

3. T.R. Shrout, H.C. Chen and L.E. Cross, "Dielectric and Piezoelectric Properties of Tungsten Bronze Lead Barium Niobate ($Pb_{1-x}Ba_xNb_2O_6$) Single Crystals," presented at the 5th European Mtg. on Ferroelectrics, Sept. 26-30, 1983, Benalmadena, Spain.

9.0 REFERENCES

1. R.B. Maciolek and S.I. Liu, J. Electronic Mat. 4, 517 (1975).

2. A.A. Ballman and H. Brown, J. Cryst. Growth 1, 311 (1967).

3. M. Kestigian and W.R. Bekebrede, Mat. Res. Bull. 8, 319 (1973).

4. J.C. Brice, O.F. Hill, P.A.C. Whifflin and J.A. Wilkinson, J. Cryst. Growth 10, 133 (1971).

5. S.T. Liu and R.B. Maciolek, J. Electronic Mat. 4, 91 (1975).

6. P.B. Lenzo, E.G. Spencer and A.A. Ballman, Appl. Phys. Lett. 18, 507 (1971).

7. A.M. Glass, J. Appl. Phys. 40, 4699 (1969).

8. R.R. Neurgaonkar,

9. K. Megumi, N. Nagatsuma, Y. Kashiwada and Y. Furuhata, J. Mat. Sci. 11, 1583 (1976).

10. K. Nagata and K. Okazaki, The Japan-US Study Seminar on Dielectric and Piezoelectric Ceramics, W-11 (1982).

11. M. Yokusuka, Jap. J. Appl. Phys. 16, 379 (1977).

12. G. Goodman, J. Am. Ceram. Soc. 36, 368 (1953).

13. G. Goodman, Am. Ceram. Bull. 31, 113 (1952).

14. R.R. Neurgaonkar, M.H. Kalisher, E.J. Staples and T.C. Lim, Proc. of Intl. Ultrasonic Symp., New Orleans, LA, 598 (1980).

15. R.R. Neurgaonkar and E.J. Staples, J. Cryst. Growth. 54, 572 (1981).

16. T.R. Shrout, L.E. Cross, P. Moses, H.A. McKinstry and R.R. Neurgaonkar, IEEE Proc. Ultrasonics Symposium, 414 (1980).

17. J.E. Geusic, H.J. Levenstein, J.J. Rubin, S. Singh and L.G. Van Uitert, Appl. Phys. Lett. 11, 269 (1967).

18. R.L. Barns, J. Appl. Cryst. 1, 290 (1968).

19. R.R. Neurgaonkar and L.E. Cross, Final Report (DARPA), Contract No. F49620-78-C-0093 (1982).

20. L.G. Van Uitert, J.J. Rubin, W.H. Grodkiewicz and W.A. Bonner, Mat. Res. Bull. 4, 63 (1969).

21. K. Nagata, T. Yamazaki and K. Okazaki, Proc. 2nd Intl. Mtg. on Ferroelectric Materials and Their Applications, 251 (1979).

22. V.V. Voronov, I.R. Dorosh, Y.S. Kusminov and N.V. Tkachenko, Sov. J. Quantum Electron. 10, 1346 (1980).

23. K. Megumi, H. Kozuka, M. Kobayashi and Y. Furahata, Appl. Phys. Lett. 30, 631 (1977).